

# An Effective Equation of State for Dense Matter with Strangeness

Shmuel Balberg and Avraham Gal

The Racah Institute of Physics

The Hebrew University, Jerusalem 91904, Israel

## Abstract

An effective equation of state which generalizes the Lattimer-Swesty equation for nuclear matter is presented for matter at supernuclear densities including strange baryons. It contains an adjustable baryon potential energy density, based on models of local potentials for the baryon-baryon interactions. The features of the equation rely on the properties of nuclei for the nucleon-nucleon interactions, and mainly on experimental data from hypernuclei for the hyperon-nucleon and hyperon-hyperon interactions. The equation is used to calculate equilibrium compositions and thermodynamic properties of high density matter with strangeness in two astrophysical contexts: neutron star matter (transparent to neutrinos) and proto-neutron star matter (opaque to neutrinos). The effective equation of state reproduces typical properties of high density matter found in theoretical microscopic models. Of these, the main result is that hyperons appear in both types of matter at about twice the nuclear saturation density, and that their appearance significantly softens the equation of state. The range of maximal masses of neutron stars found in a comprehensive parameter survey is 1.4-1.7  $M_{\odot}$ . Another typical result is that the maximal mass of a proto-neutron star with strange baryons is higher than that of an evolved neutron star (opposite to the case of nuclear matter), setting the stage for a “delayed collapse” scenario.

*PACS:* 21.30.Fe, 26.60.+c, 97.60.BW, 97.60.Jd

*Keywords:* Equation of state, Effective interactions, Strangeness in Neutron stars

# 1 Introduction

The properties of matter at supernuclear densities are a key subject of interest in the study of core-collapse supernovae and neutron stars. Theories of such matter typically predict that at the nuclear saturation density,  $\rho_s = 0.15 - 0.16 \text{ fm}^{-3}$ , it is composed of free nucleons and leptons, but at higher densities several more species of particles may appear. Chiefly among these are strange baryons, namely, the  $\Lambda$ ,  $\Sigma$  and  $\Xi$  hyperons, while  $\Delta$  baryons along with pion and kaon condensations and a deconfined-quark-phase have also been considered. The collapsed core in type II supernovae and neutron stars serve, in this sense, as cosmological laboratories for hadronic physics.

The appearance and effects of such “novel” particles in dense matter have been included in several studies in the context of neutron star structure (see for example, Refs. [1-5]). Some work has also been done regarding the collapsing core in type II supernovae [6], and recently attention has also been given to the possible impact of the appearance of strange particles in proto-neutron star evolution [7-10].

The physical state and composition of matter at high densities depends mainly on the nature of the strong interactions. However, the theoretical details of these interactions are not completely understood, and uncertainties also arise from the incompleteness of the available experimental data for nuclear matter. Such uncertainties are compounded when strange hadrons are taken into account, as relevant experimental data is rather scarce. Theoretical studies of nuclear and hadronic matter are usually performed with sophisticated models such as relativistic mean field (RMF) and Brueckner-Hartree-Fock, which involve effective Lagrangians and/or specific assumptions about baryon-baryon interactions. Some applications of these models are technically complex and often prove expensive in terms of CPU time when performing calculations at various combinations of densities and temperatures. Thus, there is also an interest in using an effective equation of state (EoS), which is analytic and depends on a small number of parameters. Such an equation will be convenient as a supplementary tool, mainly for direct use in rapid hydrodynamical simulations, and for conducting extensive parameter surveys that are necessary given the large uncertainties in the theory and experimental data regarding strong interactions.

Two commonly used effective equations of state for hot (finite temperature) nuclear matter (nucleons and leptons) are those of Lattimer and Swesty [11] and Baron, Cooperstein and Kahana [12]. In the present study we wish to construct a generalized effective equation of state for high density hadronic matter, by extending the Lattimer-Swesty (hereafter LS)

equation so as to include additional species of particles. We currently limit ourselves to strange baryons, which we view as the prime candidates for appearing in high density matter.

In Section 2 we discuss our approach for constructing the effective EoS, basing it on the formulation of local (effective) density dependent potentials for the various cases of the baryon-baryon interactions (lepton interactions are assumed to be negligible, and thus leptons are treated as non-interacting particles). Section 3 outlines the equilibrium conditions, which determine the composition and physical properties of high density matter for neutrino-free matter (neutron star) and neutrino trapped matter (core-collapse and proto-neutron-star) in beta equilibrium.

Our choice of parameters for these equations, derived mainly on the basis of hypernuclear data, is presented in Section 4; we note, that these parameters allow accurate modeling of field-theoretical interactions. We also specifically treat the consequences of recent theoretical and experimental work on  $\Sigma^-$ -atoms [13, 14], which seem to suggest a strong isoscalar repulsion in the interaction of  $\Sigma$  hyperons with a bulk of nucleons, unlike the commonly assumed interaction.

Results for the equilibrium compositions of high density matter and the corresponding EoS are presented in Section 5. These EoS's are examined with regard to the static neutron star masses they predict in Section 6. In Section 7 we offer conclusions and further discussion.

## 2 The Effective Equation of State

The construction of an effective EoS for supernuclear density matter centers on the description of the strong interaction energy. In this approach one models these interactions in some analytic form, involving a small number of parameters.

The internal energy density is approximated by dividing it into a baryon contribution, which includes kinetic, potential and mass terms, and a lepton contribution which has only kinetic and mass terms. This approximation, introduced in the LS EoS, yields the following structure of the internal energy density for supernuclear dense matter:

$$\varepsilon_{tot} = \varepsilon_{kin}(\rho, T, \{x_i\}) + \varepsilon_{pot}(\rho, \{x_i\}) + \varepsilon_{mass}(\rho, \{x_i\}) + \varepsilon_{kin}(\rho, T, \{l_i\}) + \varepsilon_{mass}(\rho, \{l_i\}), \quad (1)$$

where  $\rho$  is the total baryon density,  $T$  is the matter temperature (whose effect is handled in the kinetic energy terms),  $\{x_i\}$  and  $\{l_i\}$  are respectively the baryon and lepton fractions,  $x_i = \rho_{x_i}/\rho$ ;  $l_i = \rho_{l_i}/\rho$ . For finite temperatures, a photon contribution must be added as well.

The separation of the lepton contribution is made possible by treating leptons as non-interacting (relativistic) particles, and, as discussed in Ref. [15], electron screening effects

may be ignored because the electron-screening length is larger than the baryon separation distance.

The heart of the effective EoS is, of course, casting the potential energy density term,  $\varepsilon_{pot}$ , into an effective form. This is achieved by assuming local density dependent potentials for all strong interactions. Such a potential model must reproduce the basic features of the strong interactions, i.e. long-range attraction and short range repulsion, and - in some cases - charge dependence, compatible with isospin invariance. The most economic way to construct such a potential for the case of a single baryon of species  $y$  in bulk matter of baryon species  $x$  of number density  $\rho_x$  is:

$$V_y(\rho_x) = a_{xy}\rho_x + b_{xy}t_xt_y\rho_x + c_{xy}\rho_x^{\gamma_{xy}}. \quad (2)$$

The first term yields attraction ( $a_{xy}$  negative), the third term yields repulsion ( $c_{xy}$  positive, supposedly introducing multibody interactions), and the second (symmetry) term introduces the charge dependence through a charge (isospin)  $t$ . The common choice of parameters in effective approaches [11, 12] favors a linear density dependence of the attraction and symmetry terms, while  $\gamma_{xy}$  must be greater than unity, so that repulsion will dominate at high densities (short ranges). This formulation limits the potential energy model to at most four parameters, whose values are chosen to reproduce experimental data and accepted theoretical results. Eq. (2) can, of course, also be used for the case of a single species (i.e.,  $y=x$ ), describing the local potential felt by each baryon in the bulk of baryons of the same species.

We note that a local effective potential for the nucleon-nucleon interaction provides the basis for the well known Skyrme model (see Ref. [16] for a recent review). Similar modeling for hyperons in nuclear matter was first performed by Millener, Dover and Gal ([17], hereafter MDG), on the basis of experimental data of various  $\Lambda$ -hypernuclei, deriving a local potential for a single  $\Lambda$  in nuclear matter.

The local potential for a single baryon in a bulk of other baryons may be extrapolated into the potential energy density of bulk matter with a total density  $\rho$  that includes both types of baryons. This is done by folding  $V_y(\rho_x)$  with the partial density  $\rho_y$ , and vice versa ( $V_x(\rho_y)$  with  $\rho_x$ ), combined with weight factors (avoiding double counting of each interaction). If we choose the weight factors to be  $x/(x+y)$  and  $y/(x+y)$  respectively, the contribution of the interactions between baryons of species  $x$  and baryons of species  $y$  to the internal energy density,  $\varepsilon(x \leftrightarrow y, \rho)$  will be:

$$\varepsilon_{pot}(x \leftrightarrow y, \rho) = a_{xy}xy\rho^2 + b_{xy}t_xt_yxy\rho^2 + c_{xy} \left( \frac{x}{x+y}x^{\gamma_{xy}}y + \frac{y}{x+y}y^{\gamma_{xy}}x \right) \rho^{\gamma_{xy}+1}, \quad (3)$$

where  $x$  and  $y$  are defined as  $x=\rho_x/\rho$ ,  $y=\rho_y/\rho$ .

The above weight factors do not appear in the first two terms as they just add to unity, while in the repulsion term they retain discrimination between baryons  $y$  in matter of baryons  $x$  and baryons  $x$  in matter of baryons  $y$ . Although this form is not unique, the weight factors  $x/(x + y)$  and  $y/(x + y)$  yield the expected results in the case  $x = y$  and for the limits  $x \gg y$  and vice versa. Inherent in Eq. (3) is the neglect of possible screening effects of other baryons, so that the interaction between any two baryons is dependent only on the distance between them. This interaction may be taken as an effective average interaction between any two baryon species.

For the specific case of baryons of a single species, setting  $x = y$  in Eq. (3) requires a factor of  $\frac{1}{2}$  to avoid double counting:

$$\varepsilon_{pot}(x \leftrightarrow x, \rho) = \frac{1}{2} [a_{xx}x^2\rho^2 + b_{xx}t_x^2x^2\rho^2 + c_{xx}x^{\gamma_{xx}+1}\rho^{\gamma_{xx}+1}] . \quad (4)$$

For nucleons, charge independence is respected by choosing  $a_{nn} = a_{pp} = a_{np} \equiv a_{NN}$ , with similar relations among the symmetry and repulsion coefficients. Thus, neutrons and protons can be treated as members of a single species with the appropriate symmetry term, and we can then retrieve the potential energy density of nucleons, similar to the form presented by LS (who denote the power in the repulsion term by  $\delta$ ):

$$\varepsilon_{pot}(n, z, \rho) = \frac{1}{2} [a_{NN}(n+z)^2\rho^2 + b_{NN}(n-z)^2\rho^2 + c_{NN}(n+z)^{\delta+1}\rho^{\delta+1}] . \quad (5)$$

LS use a slightly different expression,  $a'_{NN}(n+z)^2\rho^2 + b'_{NN}nz\rho^2 + c_{NN}(n+z)^{\delta+1}\rho^{\delta+1}$ , which requires a rearrangement of the coefficients in Eq. (5). In reaching Eq. (5),  $(n-z)$  repulsive contributions were dropped so that the short-range repulsion term depends only on the total nucleon density.

We now turn to high density matter, where the hyperon species  $\Lambda$ ,  $\Sigma$  and  $\Xi$  are considered in addition to the nucleons. The full potential energy density expression will include several new terms, for the different baryon-baryon combinations:

$$\begin{aligned} \varepsilon_{pot}(\rho) = & \frac{1}{2} [a_{NN}N^2\rho^2 + b_{NN}(n-z)^2\rho^2 + c_{NN}N^{\delta+1}\rho^{\delta+1}] \\ & + a_{\Lambda N}N\Lambda\rho^2 + c_{\Lambda N} \left( \frac{N}{N+\Lambda}N^\gamma\Lambda + \frac{\Lambda}{N+\Lambda}\Lambda^\gamma N \right) \rho^{\gamma+1} \\ & + \frac{1}{2} [a_{\Lambda\Lambda}\Lambda^2\rho^2 + c_{\Lambda\Lambda}\Lambda^{\gamma+1}\rho^{\gamma+1} + a_{\Xi\Xi}\Xi^2\rho^2 + b_{\Xi\Xi}(\Xi^- - \Xi^0)^2\rho^2 + c_{\Xi\Xi}\Xi^{\gamma+1}\rho^{\gamma+1}] \\ & + a_{\Xi N}N\Xi\rho^2 + b_{\Xi N}(n-z)(\Xi^- - \Xi^0)\rho^2 + c_{\Xi N} \left( \frac{N}{N+\Xi}N^\gamma\Xi + \frac{\Xi}{N+\Xi}\Xi^\gamma N \right) \rho^{\gamma+1} \\ & + a_{\Lambda\Xi}\Xi\Lambda\rho^2 + c_{\Lambda\Xi} \left( \frac{\Lambda}{\Xi+\Lambda}\Lambda^\gamma\Xi + \frac{\Xi}{\Xi+\Lambda}\Xi^\gamma\Lambda \right) \rho^{\gamma+1} \\ & + a_{\Sigma N}N\Sigma\rho^2 + b_{\Sigma N}(n-z)(\Sigma^- - \Sigma^+)\rho^2 + c_{\Sigma N} \left( \frac{N}{N+\Sigma}N^\gamma\Sigma + \frac{\Sigma}{N+\Sigma}\Sigma^\gamma N \right) \rho^{\gamma+1} \end{aligned} \quad (6)$$

$$\begin{aligned}
& + a_{\Lambda\Sigma} \Sigma \Lambda \rho^2 + c_{\Lambda\Sigma} \left( \frac{\Sigma}{\Sigma + \Lambda} \Sigma^\gamma \Lambda + \frac{\Lambda}{\Sigma + \Lambda} \Lambda^\gamma \Sigma \right) \rho^{\gamma+1} \\
& + a_{\Sigma\Xi} \Sigma \Xi \rho^2 + b_{\Sigma\Xi} (\Xi^- - \Xi^0) (\Sigma^- - \Sigma^+) \rho^2 + c_{\Sigma\Xi} \left( \frac{\Xi}{\Xi + \Sigma} \Xi^\gamma \Sigma + \frac{\Sigma}{\Xi + \Sigma} \Sigma^\gamma \Xi \right) \rho^{\gamma+1} \\
& + \frac{1}{2} [a_{\Sigma\Sigma} \Sigma^2 \rho^2 + b_{\Sigma\Sigma} (\Sigma^- - \Sigma^+)^2 \rho^2 + c_{\Sigma\Sigma} \Sigma^{\gamma+1} \rho^{\gamma+1}] ,
\end{aligned}$$

where we define for each baryon species  $x = \rho_x / \rho$ , and introduce a shortened notation of  $N = n + z$ ;  $\Xi = \Xi^0 + \Xi^-$ ;  $\Sigma = \Sigma^+ + \Sigma^0 + \Sigma^-$ . There are no standard (isovector) symmetry terms for the  $\Lambda$  and  $\Sigma^0$  baryons, since they have zero isospin; a nonstandard (isotensor) symmetry term for  $\Sigma$ 's is disregarded. We denote the exponent of the density-dependent repulsion term for the nucleon-nucleon interaction by  $\delta$ , following LS, while all other repulsive interactions are assumed to have a common exponent  $\gamma$ , although further diversity is, of course, possible.

The kinetic energy density of the baryons contains the non-relativistic fermion kinetic energies:

$$\varepsilon_{kin}(\{x_i\}, \rho, T) = \sum_i \frac{\hbar^2 \tau_i(x_i, \rho, T)}{2m_i^*} , \quad (7)$$

where  $m_i^*$  is the density dependent effective mass of the baryons of species  $i$  (with  $c=1$ ). The entire temperature dependence of the baryon thermodynamic functions is implicitly included in this term through the Fermi functions

$$\tau_i(x_i, \rho, T) = \frac{1}{2\pi^2} \left[ \frac{2m_i^* T}{\hbar^2} \right]^{5/2} F_{3/2}(\eta(x_i, \rho, T)) \quad (8)$$

where the temperature is in units of energy (setting  $k_B = 1$ ).  $F_{3/2}$  is the corresponding Fermi integral, generally defined as

$$F_k(\eta) = \int_0^\infty u^k (1 + e^{u-\eta})^{-1} du . \quad (9)$$

The parameter  $\eta_i$  is directly related to the temperature and density through the inverse relation

$$\eta_i(x_i, \rho, T) = F_{1/2}^{-1} \left[ 2\pi^2 x_i \rho \left( \hbar^2 / 2m_i^* T \right)^{3/2} \right] . \quad (10)$$

In the case of zero temperature matter the Fermi function reduces to the simple expression  $\tau_i = \frac{3}{5} (3\pi^2 x_i \rho)^{2/3} x_i \rho$ . Typical nuclear models predict that in the depth of bulk matter the effective mass of baryons,  $m_i^*$ , will be lower than the bare mass  $m_i$ . The effective masses may be adequately represented in the Skyrme fashion

$$1/m_i^* = 1/m_i + \beta_i \rho . \quad (11)$$

The scaling parameters  $\beta_i$  arise, however, from the model of the baryonic forces, and cannot be assumed independently. The effective equation has no means to fully relate consistent

effective masses and forces (unlike RMF models where effective masses result naturally), and this point must be considered separately.

Finally, the contribution of the baryonic mass density is obviously given by

$$\varepsilon_{mass}(\{x_i\}, \rho) = \sum_i x_i \rho m_i^* . \quad (12)$$

The chemical potentials of the baryons are also immediately related to the parameter  $\eta_i$  :

$$\mu_i = \frac{\partial(\varepsilon_{tot}/\rho)}{\partial x_i} \Big|_{\{\tau_i\}, \rho} = \eta_i T + \frac{\partial((\varepsilon_{pot} + \varepsilon_{mass})/\rho)}{\partial x_i} \Big|_{\{\tau_i\}, \rho} . \quad (13)$$

In the special case of zero temperature matter  $\eta_i$  is undefined, and the chemical potentials are found by analytically differentiating  $\partial(\varepsilon_{tot}/\rho) \partial x_i$ .

Lepton contributions to the energy density are calculated through the complete (relativistic) Fermi integrals. For sufficiently high temperatures ( $T \geq 1$  MeV), the thermodynamic functions for electrons and neutrinos (when assumed to be trapped in the matter) can be approximated by the ultra-relativistic limit. Keeping the lowest order mass corrections results in the following equations for the chemical potentials [11]:

$$\rho Y_l = \frac{g_l}{6\pi^2} \left( \frac{\mu_l}{\hbar} \right)^3 \left[ 1 + \mu_l^{-2} \left( (\pi T)^2 - \frac{3}{2} m_l^2 \right) \right] \quad (14)$$

where  $m_l$  is the lepton rest mass (again in units of energy),  $g_l$  is the spin degeneracy and  $Y_l$  is the net lepton fraction per baryon (the number of particles minus the number of anti-particles). The chemical potential is then solved by

$$\begin{aligned} \mu_l &= r - q/r ; \\ r &= \left[ \sqrt{q^3 + t^2} + t \right]^{1/3} ; \quad t = 3\pi^2 \hbar^3 \rho Y_l / g_l ; \quad \text{and} \quad q = \frac{1}{3} \pi^2 T^2 - \frac{1}{2} m_l^2 . \end{aligned} \quad (15)$$

The contribution of the ultra-relativistic leptons to the total energy density for each lepton species  $l$  is given by:

$$\varepsilon_l = \frac{g_l \mu_l}{8\pi^2} \left( \frac{\mu_l}{\hbar} \right)^3 \left[ 1 + \mu_l^{-2} \left( 2\pi^2 T^2 - m_l^2 \right) + \frac{\pi^2 T^2}{\mu_l^4} \left( \frac{7}{15} \pi^2 T^2 - \frac{1}{2} m_l^2 \right) \right] . \quad (16)$$

Obviously, in zero temperature matter all formulas for the lepton thermodynamic functions reduce to simple zero-temperature fermion gas functions.

We note that the muon cannot be treated as ultra-relativistic, and its thermodynamical functions must be calculated through the corresponding Fermi integrals. However, in the case of neutrino-trapped matter muons are almost extinct (unlike the neutrino-free matter

case, where muons form at significant fractions), and we shall disregard them for the case of finite temperature matter.

The construction of the equation of state is completed by the calculation of the various contributions to the pressure in the matter. The pressure is derived from the total energy density by:

$$P = \sum_i x_i \rho \mu_i + \sum_l Y_l \rho \mu_l - f = \sum_i x_i \rho \mu_i + \sum_l Y_l \rho \mu_l + Ts - \varepsilon , \quad (17)$$

where  $f$  is the free energy density,  $f = \varepsilon - Ts$ , and  $s$  is the entropy density. Again, the pressure is composed of a baryon contribution and a lepton contribution, easy to derive from Eqs. (6)-(13) and (14)-(16) respectively. In finite temperature matter the entropy per baryon (the commonly used variable in hydrodynamical simulations),  $\tilde{s}$ , for each baryon species is

$$\tilde{s}_i = \frac{1}{\rho} \left( \frac{5\hbar^2 \tau_i}{6m_i^* T} - x_i \rho \eta_i \right) , \quad (18)$$

and for each of ultra-relativistic lepton species is

$$\tilde{s}_l = \frac{1}{\rho} \frac{g_l T \mu_l^2}{6\hbar^3} \left[ 1 + \mu_l^{-2} \left( \frac{7}{15} \pi^2 T^2 - \frac{1}{2} m_l^2 \right) \right] . \quad (19)$$

Finite temperature calculations must include a photon gas  $\mu_\gamma = 0$  contribution, with:

$$\varepsilon_\gamma = \frac{\pi^2 T^4}{15\hbar^3} ; P_\gamma = \frac{1}{3} \varepsilon_\gamma \quad \text{and} \quad \tilde{s}_\gamma = \frac{1}{\rho} \frac{4P_\gamma}{T} . \quad (20)$$

### 3 Equilibrium Conditions

The composition of the high density matter is obviously constrained by charge neutrality and baryon number conservation. Further constraints are imposed by the assumption of complete beta-equilibrium as the time scales of the weak interactions are generally much shorter than dynamical time scales in the relevant stellar systems. It is this constraint that sets most of the equilibrium conditions, as it forces all processes to take place in absolute chemical equilibrium.

The balance between baryons and leptons is maintained through beta decays. In nuclear matter, this is simply the equilibrium of the process  $p + e^- \leftrightarrow n + \nu_e$ . This equilibrium establishes the relation

$$\mu_p + \mu_e = \mu_n + \mu_{\nu_e} . \quad (21)$$

Strange baryons may form in the matter through various types of weak interactions. For example, the  $\Lambda$  hyperon can appear both in leptonic processes,  $p + e^- \rightarrow \Lambda + \nu_e$ , and in

baryonic processes such as  $n + n \rightarrow \Lambda + n$  (the inverse of which occurs in hypernuclei). There are also other possible processes, involving pions and kaons; however in this study we assume that meson condensates do not form in the matter (see discussion later in this section) and are therefore excluded. Note that the balance among strange baryons is maintained mainly through strong interactions like  $\Lambda + n \rightarrow \Sigma^- + p$ , or  $\Lambda + \Lambda \rightarrow \Xi^- + p$ . The resulting equilibrium conditions are simply that the chemical potentials of all baryons depend only on their electric charges (that determine the possible combinations in the various reactions):

$$\mu_n = \mu_\Lambda = \mu_{\Sigma^0} = \mu_{\Xi^0} ; \quad \mu_p = \mu_{\Sigma^+} ; \quad \mu_{\Sigma^-} = \mu_{\Xi^-} = 2\mu_n - \mu_p . \quad (22)$$

It is noteworthy that the chemical potentials of the negatively charged hyperons are conditioned by a larger value than the neutral ones (since dense matter is typically dominated by neutrons). For example, studies of cold high density matter usually find that the first hyperon to appear is the  $\Sigma^-$ , closely preceding the lower-mass  $\Lambda$  due to the charge difference.

The last fermion players in the high density matter are the muon and the muon neutrino. When the electron chemical potential exceeds the muon mass, muons and muon neutrinos can be formed by  $e^- \rightarrow \mu^- + \nu_e + \bar{\nu}_\mu$ , so that the equilibrium condition for the muon chemical potential is:

$$\mu_e = \mu_\mu + \mu_{\nu_e} + \mu_{\bar{\nu}_\mu} . \quad (23)$$

Eqs. (21)-(23) impose eight conditions on twelve variables, so that another four conditions are needed to uniquely determine the complete equilibrium composition of matter at given density and temperature. Two further conditions arise from charge neutrality and baryon number conservation. These conditions constrain the species fractions  $\{x_i\}$  and  $\{Y_j\}$  by

$$\sum_i x_i q_i + \sum_j Y_j q_j = 0 \quad (24)$$

where  $\{q_i\}$  are the electric charges, and

$$\sum_i x_i = 1 . \quad (25)$$

Finally, two more conditions result from the physical assumptions about the neutrino diffusion time scale. Core-collapse and proto-neutron star matter may be assumed to be opaque to neutrinos, so that neutrinos are trapped and the total lepton fraction must be kept constant. As the trapping in supernova occurs when the collapsing core reaches densities of about  $10^{12}$  gm/cm<sup>3</sup>, where no muons exist, the two resulting conditions are:

$$Y_e + Y_{\nu_e} = Y_l = \text{const} ; \quad Y_\mu + Y_{\nu_\mu} = 0 \quad (26)$$

where  $Y_l$  is determined at the onset of trapping at about 0.35-0.4, with  $Y_e/Y_{\nu_e} \approx 5 - 7$ , depending on the exact trapping density (see Bethe's detailed review [18]). As mentioned

earlier, we will ignore the minute muon production in proto-neutron-star in this study. Neutron star matter, on the other hand, is completely transparent to neutrinos (the transparency settles after about 50 seconds of proto-neutron-star evolution [19]), and the neutrino chemical potentials are set to zero. Muons are then easier to create (the threshold condition for muon creation is simply  $\mu_e = m_\mu$ ), but the total lepton density is not constrained. Neutron star matter is considerably deleptonized with respect to the proto-neutron star. The two equilibrium conditions are:

$$\mu_e = \mu_\mu \quad ; \quad \mu_{\nu_e} = \mu_{\nu_\mu} = 0 \quad , \quad (27)$$

and all the chemical potentials can be expressed as linear combinations of the electron and neutron chemical potentials (associated with the electric and baryonic charges, respectively).

Solving the complete set of conditions yields the equilibrium fractions of the baryon and lepton species for any given density and temperature. The effective form of our EoS enables a low-order Newton-Raphson iteration process, which is quick and efficient. The equilibrium compositions and the resulting thermodynamic properties are then calculated for the large variety of strong interaction parameterizations discussed below.

Other particle candidates for appearance in the high density matter are the  $\Delta$  isobars and  $\pi$  and  $K$  mesons as condensates. Current theories predict  $\pi N$  S-wave repulsive forces which exclude pion condensates, and indirectly, make the formation of  $\Delta$ 's unfavorable as well [3, 10]. However, as shown by Weber and Weigel [20], in Relativistic-Hartree-Fock calculations some evaluations of the  $\rho N \Delta$  coupling enhance the formation of the  $\Delta^-$ . Kaon and anti-kaon condensation has attracted considerable attention [21], but some recent investigations (see, for example, Refs. [5, 22]) do not find kaon effective masses dropping low enough at relevant densities. Clearly, the formation of hyperons in the matter will further suppress meson condensation [5, 4]. We therefore opt not to include  $\Delta$ 's and meson condensates in this study; further generalization is, of course, possible, where the model dependence of the above arguments may be examined. A final issue is that of the transition into a deconfined quark phase: at some high density the hadronic identities of the quark states must begin to fade, as the baryons will overlap. In this study we do not treat quark degrees of freedom, and allow the baryonic effective equation of state to dominate up to  $8\rho_s$ . Quark degrees of freedom, however, might come into effect at lower values of density (an especially exotic case is the possibility of stable strange quark matter, which leads to the existence of strange stars [23]). The issue of quark deconfinement is deferred to a future work.

## 4 Choice of Parameters

The local potential approach requires four parameters for every combination of baryon-baryon interactions in Eq. (6): the coefficients  $a, b, c$  and the density power dependence  $\gamma$  ( $\delta$  for the nucleon-nucleon case). The effective masses of the baryons, or rather their density dependence through the parameters  $\beta_i$  defined in Eq. (11), are required as well.

In principle, all parameters of the local potentials could be determined experimentally, but in practice there are large uncertainties due to limited experimental data, and some values must be drawn from theory. The experimental and theoretical data used as basis for evaluating the parameters are discussed briefly in the proceeding paragraphs.

### 4.1 Nucleon-Nucleon Interactions

The properties of the nucleon interactions at the nuclear saturation density,  $\rho_s$ , are measured to a reasonable precision in finite nuclei. The experimental value of this density is estimated to be in the range  $0.145\text{--}0.17\text{ fm}^{-3}$ , and in this study we follow LS by employing the Skyrme I' force value of  $\rho_s = 0.155\text{ fm}^{-3}$ .

As shown in LS, the values of the parameters  $a_{NN}, b_{NN}, c_{NN}$  and  $\delta$  are evaluated from the binding energy, symmetry energy and incompressibility of saturated symmetric nuclear matter, derived from typical experimental results and the Skyrme model (see Section 2.2 of LS for detail). However, the parameters  $a_{NN}, c_{NN}$  and  $\delta$  strongly depend on the nuclear incompressibility which is poorly determined in finite nuclei, and is difficult to match with theoretical predictions (which generally yield too high incompressibility). Thus, quantifying the properties of the nucleon-nucleon interactions at high densities leaves a large range of uncertainty, especially for  $\delta$ , which as a result may be set practically arbitrarily between unity and about 2. For example, LS use the Skyrme value of the incompressibility  $K_s = 375\text{ MeV}$ , leading to  $\delta = 2.002$ , but in a later work [24] values down to  $K_s = 180\text{ MeV}$ , resulting in  $\delta = 1.07$  are also considered. In order to investigate the model dependence due to this parameter, we will examine the values  $\delta = 2, \frac{5}{3}$  and  $\frac{4}{3}$ . The appropriate values for the parameters  $a_{NN}, b_{NN}$  and  $c_{NN}$  for these values of  $\delta$  are presented in Table 1.

### 4.2 Hyperon-Nucleon Interactions

Experimental data of effective nucleon-hyperon interactions are confined to hypernuclei (for a recent review, see [25]). This clearly limits the interpretation of the data, and requires a

combination of experimental and theoretical analysis.

There is a considerable body of information on binding energies,  $B_\Lambda$ , of  $\Lambda$ 's bound in various single particle orbitals in hypernuclei with total baryonic number from  $A = 3$  to  $A = 208$ . By analyzing these data in a Skyrme-Hartree-Fock picture MDG determined a well depth of

$$-V_\Lambda(\rho_N = \rho_s) \approx 27 - 28 \text{ MeV} , \quad (28)$$

defined as the potential seen by a single  $\Lambda$  in nuclear matter at saturation density, which is roughly  $\frac{1}{3}$  of the nucleon well depth in a similar parameterization. Constraining the local potential by the well depth at nuclear saturation density is the equivalent of using the bulk binding energy to constrain the nucleon-nucleon interaction (related to the well depth through the Fermi kinetic energy). By combining the data for many hypernuclei, MDG used the  $A$  dependence to evaluate the  $\Lambda$ -nuclear potential for densities  $\rho \leq \rho_s$  and fitted a local potential of the form  $V_\Lambda(\rho_N) = a\rho_N + c\rho_N^\gamma$  to the experimental results, deducing  $a$  and  $c$  for a given  $\gamma$ . MDG achieved reasonable fits for the single  $\Lambda$  orbitals in ordinary hypernuclei, but - again - could not constrain the shape of the potential for the high density regime, and therefore could not uniquely determine the exponent  $\gamma$  of the repulsion term. Several possible choices for the parameters  $a, c$  and  $\gamma$  are presented in Table 2 below. Figure 1, reproduced from MDG, demonstrates the character of the uncertainties of the baryon interactions, as inherent in the local potential formulation. The single  $\Lambda$  local potential in nuclear matter,  $V_\Lambda(\rho_N)$ , is plotted against the nuclear matter density, for different choices of the exponent  $\gamma$ . All the potentials are constrained by a well depth of about  $-28$  MeV at nuclear saturation density and the  $\Lambda$ -hypernuclear binding energies for lower densities, so that all the plots yield similar results for  $\rho \leq \rho_s$ . However, the unconstrained behavior at high density is quite divergent, depending strongly on the value of  $\gamma$ . For example, the cross-over density,  $\rho_{co}$  for which  $V_\Lambda(\rho_{co}) = 0$  varies from about  $\rho_{co} = 2\rho_s$  for  $\gamma = 2$  to  $\rho_{co} = 3.5\rho_s$  for  $\gamma = \frac{4}{3}$ . It is noteworthy that this local potential does reproduce the calculated single particle potentials found in RMF models [30].

Experimental data of  $\Sigma$  hypernuclei are more ambiguous, partly because of the strong  $\Sigma N \rightarrow \Lambda N$  decay channel. It is common to assume that the  $\Sigma$  well depth is equal to that of the  $\Lambda$  [26]. The isospin dependent component of the interaction of a  $\Sigma$  hyperon in nuclear matter ( $\Sigma$ -nm) is usually evaluated from theory, typically predicting a  $\Sigma$  isovector coupling constant (due to the  $\rho$  meson field in RMF models) of the same order of magnitude as for nucleons. Possible choices for the parameters  $a, b, c$  and  $\gamma$  then follow from Tables 1 and 2, and are presented in Table 3. However, a recent analysis [13, 14] of theoretical work and experimental data concerning  $\Sigma^-$ -atoms suggests that there is a strong isoscalar repulsion in the  $\Sigma$ -nm interaction. These studies, which also determine the isovector component of the  $\Sigma^-$ -nucleus interaction, indicate that  $\Sigma$  baryons are strongly repulsed in the nuclear

interior. A corresponding density dependent local potential has also been proposed (again with difficulty in determining the high power density dependence) for  $\Sigma^-$  hyperons:

$$2\mu V_\Sigma(\rho_N) = -4\pi \left(1 + \frac{\mu}{m}\right) \left\{ \left[ b_0 + B_0 \left(\frac{\rho_N}{\rho_s}\right)^\alpha \right] + \left[ b_1 + B_1 \left(\frac{\rho_N}{\rho_s}\right)^\alpha \right] (n - z) \right\} \rho_N , \quad (29)$$

where  $\mu$  is the  $\Sigma$ -nucleus reduced mass (for nuclear matter it is simply the  $\Sigma$  mass) and  $m$  is the nucleon mass. The  $(b_0, B_0)$  term describes the isoscalar component of the interaction, and with  $B_0 < 0$  and  $|B_0| > b_0$  a strong repulsion is produced in the nuclear interior. The second term introduces isospin dependence, reversing sign for the  $\Sigma^+$ . The real part of this potential may be taken as the  $\Sigma$ -nm interaction for equilibrium purposes, as the imaginary part represents mainly the  $\Sigma N \rightarrow \Lambda N$  channel. A representative set of parameters for Eq. (29) is given in Table 4. We investigate both of the possibilities listed in Tables 3 and 4 for the  $\Sigma$ -nm interaction in constructing the equation of state.

In emulsion experiments with  $K^-$  beams there are a few events attributed to the formation of  $\Xi$ -hypernuclei. Although the evidence is far from being compelling, the data can be interpreted [27] consistently in terms of a potential well depth of

$$-V_\Xi(\rho_N = \rho_s) \approx 20 - 25 \text{ MeV} . \quad (30)$$

Such a result has also been derived in one-boson-exchange (OBE) models [26]. The isospin component of the  $\Xi N$  interaction is very model dependent, ranging from negligible [26] (an order of magnitude smaller than that observed for nucleons) to equal to that of nucleons [5]. Possible choices for the parameters  $a, c$  and  $\gamma$ , assuming  $b_{\Xi N} = 0$  are listed in Table 5. In deriving these parameters we assumed  $-V_\Xi(\rho_N = \rho_s) = 24$  MeV for symmetric nuclear matter (where symmetry terms vanish) and that for a given value of  $\gamma$  the crossover density,  $\rho_{co}$ , for which  $V_\Xi(\rho_N = \rho_{co}) = 0$  is equal to that for  $\Lambda$  in nuclear matter, thus simulating universality in the high density regime.

### 4.3 Hyperon-Hyperon Interactions

The experimental data regarding hyperon-hyperon interactions is extremely scarce. There are a few events which may be interpreted by the creation of  $\Lambda\Lambda$  hypernuclei (see Ref. [25]). Analysis of these events requires a rather strong  $\Lambda\Lambda$  attraction, which is not easily reproduced by theory [29]. Recent studies with RMF models remedied the hyperon-hyperon interaction by adding two mesons [5, 28] which couple only to the hyperons. Schaffner et al. [28] constructed single particle potentials on the basis of OBE calculations of the Nijmegen group, and estimated the well depths of hyperons in hyperon matter as follows:

$$-V_{h_1}(\rho_{h_2} = \rho_s) = 40 \text{ MeV} , \quad (31)$$

implying a universal hyperon-hyperon interaction. Similar to the case of the  $\Xi$ -nm interaction, the coefficients  $a_{h_1 h_2}$  and  $c_{h_1 h_2}$  can be determined for a given value of  $\gamma$  by requiring that for symmetric matter the potential depth at a density equal to the nuclear saturation density be equal to the value assumed in Eq. (31), and that the crossover density for which the potential is zero, be equal to that of the  $\Lambda$  in nuclear matter ( $\Lambda$ -nm) case. The appropriate values for the inter-hyperon interactions are given in Table 6.

Generally, the symmetry coefficients  $b_{xy}$  in Eq. (6) are independent of  $\gamma$ , and must be determined separately. The isospin dependent components of the hyperon-hyperon interaction must be drawn from theory. As mentioned earlier, the isovector coupling constant of the  $\Sigma$  baryons is typically assumed to be up to twice that of the nucleons, while that of the  $\Xi$  baryons is unclear. We assumed that only the N-nm,  $\Sigma$ -nm and  $\Sigma$ - $\Sigma$ m interactions have a nonzero isospin component, and the corresponding values of the symmetry coefficients are presented in Tables 1, 3 and 6.

We conclude this discussion by reemphasizing the large uncertainties surrounding the baryon-baryon interactions, especially regarding the density dependence. Constraining the local potentials in nuclear matter by assuming a given well depth at saturation density does not limit the shape of the potential at higher densities, which is handled in the local potential forms of Eq. (6) by the parameters  $\gamma$  and  $\delta$ . We therefore treat the exponents  $\gamma$  and  $\delta$  as free variables, and simply assume a universal nature to all multibody forces, so that we may also set  $\gamma=\delta$ .

The evaluation of the baryon effective masses is a fundamental problem in any analysis of supernuclear density matter. The values of effective masses are needed for the kinetic and mass energy density terms of Eqs. (7) and (12) respectively, and nuclear matter calculations typically predict [16] that the nucleon mass in bulk matter is smaller than the bare mass by a factor of  $m^*/m \approx 0.7$  at saturation density, and will continue to decrease for higher densities, due to both interaction and relativistic effects. The analysis of the effective masses of all the baryons in [5] yields similar results for nucleons and hyperons alike.

The local potential has no mechanism to generate both the interactions and the effective masses consistently. LS chose to set  $m^*/m = 1$ , which is a reasonable approximation for densities up to about twice the nuclear saturation density (and may also be justified by some uncertainties regarding effective masses at the Fermi surface [31]). At higher densities such an approximation becomes questionable. While the explicitly density dependent interactions in the potential model may compensate for some of the expected decrease in the effective masses (LS include a further explicit dependence of the forces on the assumed values for the

effective masses - see Eqs. (2.20-21) in LS), relativistic effects are not taken into account.

For lack of a better model, in this work we will use  $m^*/m = 1$ . An obvious flaw in setting all effective masses equal to the bare ones is that mass differences between the various types of baryons remain constant. Theory clearly suggests otherwise (see, for example, Figs. 4 and 7 in [5]), and changing the mass differences will clearly affect the equilibrium compositions. For example, theory predicts that the effective mass of nucleons in nuclear matter at  $\rho = \rho_s$  is  $m_N^*/m_N \approx 0.55 - 0.7$ , while that of the  $\Lambda$  decreases only to  $m_\Lambda^*/m_\Lambda \approx 0.8$  [17]; hence the mass difference will be larger than for the bare masses (and  $\Lambda$ 's will form in nuclear matter at higher densities than for  $m^*/m = 1$ ). The sensitivity of the results to this crude assumption can be examined by using nonzero positive values for the coefficients  $\beta_i$  of Eq. (11), which will yield effective mass functions similar to those found in RMF models (for example, in Refs. [5, 9]).

## 5 Results: Equilibrium Compositions and Equations of State

The basic features of the dense matter are the different particle fractions and the equation of state, both of which are dependent on the baryon density of the matter, and of the modeling of the strong interactions. In this Section the equilibrium compositions and equations of state are examined and compared for the different cases of candidate hyperon species (no hyperons,  $\Lambda$ 's,  $\Sigma$ 's and  $\Xi$ 's, and only  $\Lambda$ 's and  $\Xi$ 's but no  $\Sigma$ 's when assuming a repulsive  $\Sigma$ -nm interaction). The sensitivity to the choice of parameters of the baryon-baryon interactions is also examined, by setting different values for the exponents  $\delta$  and  $\gamma$ .

We shall focus on the simpler case of neutron star matter, which can be well approximated as being at zero temperature, where all thermodynamic functions are easily found. Some results regarding proto-neutron-star (core-collapse) matter are presented in the latter part of this Section, where the assumed thermodynamic conditions are detailed.

### 5.1 Neutron Star Matter

Neutron star matter may be well approximated as having zero temperature, since evolved neutron stars have internal temperatures considerably below 1 MeV. The internal energy density  $\epsilon$  and the free energy density  $f$  are identically the same, and the kinetic energy terms in Eqs. (7,8) are all simply related to the Fermi momenta.

Shown in Fig. 2 are the particle fractions versus the baryon density for matter containing neutrons, protons electrons and muons, calculated by using the parameters for  $\delta = 2$  (see Table 1), and ignoring the possible appearance of hyperons. Compositions are calculated up to about  $8\rho_s$ , where quark degrees of freedom are assumed to come into effect, and the validity of a baryonic model of the matter becomes questionable. These plots are very similar to those calculated in various models of nuclear matter for neutron stars. The main features of such matter are:

1. Neutrons are by far the dominant species in the matter.
2. Both electrons and muons are present in the matter. At increasing densities the chemical potential of the leptons rises (due to the rising Fermi energies), and the muon fraction approaches that of electrons, as the Fermi energies drive the chemical potential up so that the mass difference is of lesser significance.
3. The balance of nucleons and leptons is determined by the difference  $\mu_n - \mu_p$  (commonly denoted as  $\hat{\mu}$ ) and by  $\mu_e$ . Equilibrium demands that both be equal, but since  $\mu_n - \mu_p$  has a steeper density dependence, there is some decrease in the neutron fraction and some increase in the proton and total lepton fractions as a function of the total baryon densities.

These features are common to a variety of nuclear matter models and are only weakly model dependent. This results in similar graphs for the other parameterizations; although specific details are, of course, model dependent (for example, the exact proton fraction which is highly important for direct Urca cooling rates).

The picture clearly changes when hyperons are taken into account. Figures 3a, 3b and 3c show the various particle fractions as a function of the total baryon density for  $\gamma = \delta = 2, \frac{5}{3}$  and  $\frac{4}{3}$  respectively. In all cases the hyperon-hyperon well depth was set as  $-40$  MeV, and the  $\Sigma$ -nm interaction is assumed to be equal to the  $\Lambda$ -nm one (except for the symmetry term, which is nonzero for  $\Sigma$ 's and nucleons). The appearance of hyperons affects all the main features of the equilibrium compositions. The key effects to be noted are:

1. In all cases hyperons appear at about twice the nuclear saturation density, and at densities of about  $2.5\rho_s$  they sustain a significant fraction of the total baryon population.
2. The first hyperon species to appear is the  $\Sigma^-$ , closely followed by the  $\Lambda$ . The negative charge of the  $\Sigma^-$  outweighs the 80 MeV mass difference, as a result of the more lenient condition, Eq. (22), for its chemical potential. However, the formation of  $\Sigma^-$  hyperons is quickly moderated by the charge dependent forces, which disfavor an excess of  $\Sigma^-$ 's over  $\Sigma^+$ 's, and a joint excess of  $\Sigma^-$ 's and neutrons. Thus the  $\Sigma^-$  fraction saturates at

about 0.1, while the  $\Lambda$ 's, free of charge-dependent forces, continue to accumulate until the repulsive (multibody) forces bring saturation on them as well.

3. All other hyperon species follow, and appear one by one in the matter. With the assumptions mentioned above,  $\Sigma$ 's generally appear before the  $\Xi$ 's due to the large mass difference, but the  $\Xi^-$  becomes favored due to its negative electric charge, and quickly becomes abundant in the matter. Since we assume no charge-dependent forces for the  $\Xi$  baryons, the  $\Xi^-$  fraction does not saturate quickly, and its fraction overtakes that of the  $\Sigma^-$  at high densities.
4. A unique aspect of hyperon appearance in all cases is the immediate deleptonization of the matter. Leptons are rather expensive in terms of energy density (and pressure), surviving in nuclear matter only because of the need for charge neutrality and because the charge-dependent forces impose a significant proton fraction. Hyperons create an option for lowering the neutron excess free of lepton formation, and the negatively charged hyperons allow charge neutrality to be maintained within the baryon community. Thus, the increase of the lepton abundance is cut short by the formation of the hyperons and, in some cases, the appearance of the  $\Xi^-$  is followed by a very powerful deleptonization. For  $\gamma = \delta \geq \frac{5}{3}$  the muon population is even completely extinguished (obviously, the  $\Sigma^-$ 's cannot achieve this alone because of their saturation fraction, imposed by the symmetry forces). The case of  $\gamma = \delta = \frac{4}{3}$  is somewhat eccentric, maintaining a high lepton content along with the rather moderated appearance of hyperons. This is a consequence of setting  $\delta = \frac{4}{3}$ , which represents a too mild increase in the nucleon-nucleon repulsion with increasing density, thus suppressing hyperon production. Such a composition seems to be unlikely, since a combination of hyperons and a high lepton content will create very rapid cooling rates [32-35].

Some model dependence does exist, of course, as weaker nucleon repulsion is necessarily accompanied by less hyperon production. For  $\delta = 2$ , hyperon production is so favorable that at high densities  $\Lambda$ 's, not neutrons, are the most abundant species, while for  $\delta = \frac{4}{3}$  nucleons dominate the matter even at  $8\rho_s$ . The appearance of hyperons other than  $\Sigma^-$  and  $\Lambda$  is also somewhat model dependent: the more powerful the high density repulsion (among nucleons and hyperons), the formation of  $\Sigma^0$  and even  $\Sigma^+$  becomes more favorable at sufficiently low densities, where the more massive  $\Xi^-$  is still absent; for weaker repulsion, it is the  $\Xi^-$  which appears first of the three, at densities where the effect of its negative charge is sufficient to overcome the 120 MeV mass difference.  $\Xi^0$ 's appear only when repulsive forces become dominant again and the introduction of more species is thus more effective in lowering the potential energy density.

The reason for the hyperon formation density being only weakly model dependent is that

when hyperons are excluded, the nucleon chemical potentials in nuclear matter rise steeply with density. All models predict that at about  $2\rho_s$  the nucleon-nucleon interaction is far beyond maximum attraction, and in some models it is already repulsive, so that lowering the partial density of the nucleons is clearly favorable. Thus, although the exact density for hyperon appearance is model dependent, it does not vary by more than a few hundredths of a fm<sup>-3</sup>. We note that this is also the reason for the quick rise in the hyperon fractions with density after formation. The only balance to this trend are the kinetic energies, which are far outweighed until the hyperon fraction rises to the order of about 0.1. This behavior is less pronounced for the  $\Sigma$ 's than for the  $\Lambda$ 's (and in our model, also for the  $\Xi$ 's) because of the nonzero symmetry term, which disfavors a fast build-up of one species.

When using the effective equation of state, the effects discussed above tend to overshoot, creating non-monotonic irregularities in the curves (most notable in the proton and lepton fractions). This (unphysical) effect is moderated to large extent in RMF models, which add further control through the effective masses which are density and species-fraction dependent.

Generally, Figs. 3a and 3b show a fair agreement with the results of the equilibrium compositions found in the mean field calculations of [3-5]. This agreement suggests that the effective equation of state can indeed be considered as a trustworthy tool in the analysis of high density baryonic matter. The somewhat eccentric case of  $\gamma = \delta = \frac{4}{3}$  examined in Fig. 3c, however, is qualitatively different from the RMF results. It seems that this case should be treated with some suspicion, although we will keep it in the analysis below. It is noteworthy that the quantitative details of the compositions are model dependent in the RMF calculations as well. For example, the deleptonization rate and other features of the PL-Z model in Ref. [5] resemble our  $\gamma = \delta = 2$  case, while those of case 2 in Ref. [3] (which is relevant for our discussion) bear higher resemblance to the  $\gamma = \delta = \frac{5}{3}$  case.

We now turn to the case of strong isoscalar repulsion in the  $\Sigma$ -nm interaction, suggested in [13, 14]. Using the local potential of Eq. (29) with the parameters listed in Table 4 (or any of the other sets of parameters in [13] that fit the experimental data of  $\Sigma^-$ -atoms) yields a repulsive potential of the order of tens of MeV's for  $\Sigma$ 's in nuclear matter at saturation density, and even greater repulsion at higher densities.  $\Sigma$  hyperons are thus disfavored in nuclear matter, and the obvious byproduct is the exclusion of these species in the high density matter under discussion.

Figures 4a, 4b and 4c show the various particle fractions as a function of the total baryon density for  $\gamma = \delta = 2, \frac{5}{3}$  and  $\frac{4}{3}$  respectively, when the hyperon-hyperon potential well depth is set as  $-40$  MeV, and the  $\Sigma$ -nm interaction is constrained by fitting to the  $\Sigma^-$ -atoms data. Clearly,  $\Sigma$  hyperons are absent, but other than this, the key features of hyperon formation are unchanged:

1. Hyperons appear again at about twice the saturation density, and at about  $2.5\rho_s$  the hyperon fraction is already significant. In this case, however, the entire effect is due to formation of  $\Lambda$ 's. This quantitative result is practically model independent. The appearance of the  $\Lambda$ 's halts the increase in the lepton population, and when  $\Xi^-$ 's are added further deleptonization occurs. The  $\Lambda$  actually appears at lower densities than it did when  $\Sigma$ 's were present, since now it has no competition from the  $\Sigma^-$ .
2. The  $\Xi^-$  appears as well in all cases, at slightly lower densities than for the corresponding case when competing with  $\Sigma$ 's. The formation of  $\Xi^0$  is model dependent, again, since stronger high density repulsion favors the introduction of more species.

The total hyperon fraction is again highly model dependent as are the specific details of the deleptonization.

The sensitivity of the results to the assumed value of the hyperon-hyperon well depth, is examined by setting its value to zero - “turning off” the hyperon-hyperon interaction (with the exception of the  $\Sigma$ - $\Sigma m$  symmetry term, which is kept unchanged). Fig. 5 presents the equilibrium compositions found for the  $\gamma = \delta = 2$  case when all baryon species are allowed (assuming the  $\Sigma$ - $nm$  interaction to be equal to the  $\Lambda$ - $nm$  one) for a zero hyperon-hyperon well depth (while all other parameters are unchanged). The considerable similarity to the compositions for the corresponding case with a relatively large hyperon-hyperon well depth (Fig. 3a) is clear. There is a slight moderation in the rate of accumulation of hyperons (missing the attractive interactions among hyperons of the same species at small partial densities) while the appearance of the more massive hyperons is somewhat delayed, because there is also no repulsion among the abundant hyperons. These effects are visible but clearly are of second order, since the matter is dominated by nucleons in most of the density range, so it is the nucleon-nucleon and hyperon-nucleon interactions which determine the equilibrium compositions. The sensitivity to the hyperon-hyperon interaction is even weaker for lower values of  $\delta$  and  $\gamma$ , as the nucleon fraction in these cases is larger. A similar relative insensitivity to the hyperon-hyperon well depth is found also when  $\Sigma$ 's are excluded from the matter.

The solution for the equilibrium compositions enables the determination of the thermodynamic functions, explicitly the energy density and the pressure, for constructing the EoS. The key point regarding the effect of introducing extra particle species into the matter in this respect is the softening of the EoS. This softening is the consequence of turning potential and kinetic energy of the already present baryons into masses of the new species, and in reducing repulsion (and sometimes even gaining attraction) in the potential energy terms, due to the lowering of the partial densities of the abundant species. These two effects lower

the energy density (so that the mass-energy density at a given baryon density is somewhat less than the corresponding energy density of nuclear matter at the same baryon density), but the main effect involves the pressure, since storing energy in mass is cheapest in terms of pressure. The decrease of the lepton population does add further softening, but this effect is of second order.

The nature of the EoS is thus dependent on the number of species, in addition to the obvious dependence on the baryon-baryon interaction model. It is instructive to begin with the resulting EoS for nuclear matter for the three cases corresponding to  $\delta = 2, \frac{5}{3}$  and  $\frac{4}{3}$ , plotted in Fig. 6. Since no hyperons are considered, the resulting EoS is a direct function of the nuclear interaction model, namely, of the value of  $\delta$ . The differences between the three equations are clearly visible. It is noteworthy that the  $\delta = 2, \frac{5}{3}$  equations break the causality limit ( $(dP/d\varepsilon) \leq c^2$ ) at some density, where the plots are made dashed. This is a known flaw in effective models for the nuclear interactions, sometimes amended by introducing a finite-range into the local potentials.

The properties of the EoS change qualitatively when hyperons are taken into account: Fig. 7 shows the resulting EoS for three types of matter with  $\delta = \gamma = \frac{5}{3}$ , for a hyperon well depth of  $-V_{h_1 h_2} = 40$  MeV. The three cases are 1) nuclear matter (n-p-e- $\mu$ ); 2) baryon matter including  $\Lambda$ 's and  $\Xi$ 's but no  $\Sigma$ 's (assuming a repulsive  $\Sigma$ -nm interaction [13]); and 3) all eight species of baryons appear. The three plots demonstrate clearly the softening of the EoS when hyperons are included, this softening becoming more pronounced when the  $\Sigma$ 's are also included.

We must note that the numerical peaks in the particle fractions discussed above are unfortunately carried over to the EoS, when the unphysical fast rise in the  $\Lambda$  fraction (and sometimes the  $\Xi^-$  fraction as well) yields a slight dip in the pressure, so that over a small region the unphysical result of  $\partial P/\partial\varepsilon < 0$  is obtained. By employing a mathematical smoothing scheme, interpolating the pressure-density dependence in these small regions, we are able to amend this shortcoming, particularly for the case of  $\gamma = 2$ .

Fig. 8 compares the resulting equation of state for three cases of the baryon-baryon interactions, i.e.  $\gamma = \delta = 2, \frac{5}{3}$  and  $\frac{4}{3}$ , and in all cases the hyperon-hyperon well depth is assumed to be  $-V_{h_1 h_2} = 40$  MeV, and the  $\Sigma$ -nm interaction is assumed to be equal to the  $\Lambda$ -nm one. It is noteworthy that all three equations of state are quantitatively similar, indicating a rather weak dependence on the precise description of the short-range forces represented by the exponents  $\delta$  and  $\gamma$ . A similar trend is found when a highly repulsive  $\Sigma$ -nm interaction is assumed, with all equations being somewhat stiffer than the corresponding cases where the  $\Sigma$ 's are allowed in the matter. Thus, an important feature of our results is that the equation of state is much less sensitive to the details of the baryon-baryon interaction, with

the obvious exception of the two extreme possibilities for the  $\Sigma$ -nm interaction.

The nucleon-nucleon interaction, which determines the stiffness of the nuclear-matter equation of state, also determines the rate at which the nucleon chemical potential rises with increasing density. A greater rise in the nucleon chemical potential is the incentive to enhanced formation of hyperons in the matter, which in turn softens the total equation of state. *Our key observation is that the macroscopic properties of the equation of state are thus strongly coupled to the microscopic equilibrium compositions, and once hyperons are available the resulting equation of state is constrained to a significantly narrower range of values.* We may conclude that *hyperons serve as a “pressure control” mechanism* in high density matter, and its nature depends mainly on the number of hyperon species available.

Explicitly, as long as attractive nucleon-nucleon and nucleon-hyperon well depths are assumed, the resulting EoS is only mildly sensitive to the choice of  $\delta$  and  $\gamma$ . This is mainly reflected in the width of the “semi-plateau” region, where the pressure grows only very mildly: the greater the value of the exponents, the higher the relative gain  $|dV/d\rho|$  in attraction at low densities and the wider the density range where the hyperon appearance, mainly of the  $\Lambda$ , creates the “semi-plateau” region. On the other hand, if a large value is chosen for the exponents, there is also a steeper rise of repulsion at higher densities, which builds up the pressure faster. These two effects are balanced by the appearance of new species in the matter, when such species are available. New species will appear when the pressure (and internal energy) rise steeply with the baryon density, but their appearance is delayed when the species already present moderate the pressure build up, as happens in the “semi-plateau” regions.

The softening of the EoS may be demonstrated by calculating the adiabatic index  $\Gamma = \varepsilon/P\partial(P)/\partial(\varepsilon)$ . Fig. 9 shows the adiabatic index as a function of the mass energy density, for nuclear matter and for matter containing nucleons and hyperons, with  $\delta = \gamma = \frac{5}{3}$ . The appearance of the hyperons is easily identified, as each of them lowered the adiabatic index as long as its fraction did not saturate. The  $\Lambda$ ’s and  $\Xi$ ’s cause greater “dips” in the value of  $\Gamma$  than the  $\Sigma$ ’s, since their formation is not moderated by charge dependent forces.

The sensitivity of the “pressure control” to the hyperon-hyperon interaction is found to be especially weak, since the matter is nucleon dominated in at least most of the relevant density range (and for  $\gamma = \delta = \frac{4}{3}$  even for the entire range). The deeper  $V_{h_1 h_2}$  is, there will be a stronger hyperon-hyperon attraction at low partial densities (further favoring hyperon production), but also a stronger hyperon-hyperon repulsion at high partial densities. Hence, through most of the density range the hyperon fractions quickly saturate so that their contribution to the energy density (and pressure) are relatively independent of the details of the hyperon-hyperon interaction.

We comment briefly on the issue of the effective masses. Several equilibrium compositions were recalculated with baryon effective masses  $m^*/m \leq 1$  derived by using nonzero values for the coefficients  $\beta_i$  in Eq. (11). We find that as long as the mass differences between the various baryon species do not change considerably from the case of bare masses, the equilibrium compositions are very similar to those found by using  $m^*/m = 1$ . This is a natural result, since the chemical potentials are highly density dependent through the potential energy terms, and so the densities at which hyperons appear do not vary by more than a few hundredths of  $\text{fm}^{-3}$ . The corresponding equations of state are more sensitive to the values of the effective masses, requiring some careful consideration. We find that the pressure vs. baryon density is only mildly dependent on the precise choices for  $m^*/m$ , and the basic feature of hyperon induced “pressure control” is maintained. Since the mass density gives a large contribution to the energy density, the pressure vs. energy density relation is more complicated when effective masses are used (and, indeed, LS scale their energy density relative to the neutron effective mass). However, if the energy density is scaled so that for nuclear matter at nuclear saturation density it yields the typical value of  $\varepsilon(\rho_N = \rho_s) \approx 2.4 \times 10^{14} \text{ gm/cm}^3$ , the resulting equations of state are once again approximately similar to those found for  $m^*/m = 1$ . In summary, we believe that the equations of state found using  $m^*/m = 1$  reasonably reflect the gross properties of the equations of state that are calculated with finer approximations regarding the effective masses.

## 5.2 Proto-Neutron Star Matter

The physical conditions in proto-neutron star matter basically differ from those in fully-evolved neutron star matter in two main features: the temperature is of the order of 10 MeV and more, so it must be treated as finite, and - to a reasonable approximation - the matter is opaque to neutrinos, trapping them and keeping the total lepton fraction,  $Y_l$ , constant.

Both of these general considerations affect the equilibrium composition as well as the equation of state of the high density matter. Finite temperature means also finite entropy, which will stiffen the EoS of matter for a given composition [9] and broaden the population levels of the baryon species, thus lowering the chemical potentials. A constant lepton fraction imposes a much higher electron fraction than in neutron star matter, clearly affecting the baryon species composition, and through it the EoS. Generally, studies of core-collapse and proto-neutron matter with finite temperature and a constant lepton fraction point to the latter as the more important of the two. Its value is determined by the onset of neutrino trapping in the collapsing core of the supernova, and is usually found to be  $Y_l = 0.3 - 0.4$  [18]; in this Section we use the value of 0.36. The temperature is typically constrained by the entropy

per baryon,  $\tilde{s}$ , which tends to be constant throughout the star. We use a temperature of  $T = 20$  MeV, which is about equivalent to  $\tilde{s} \approx 2$  [9].

Once more we begin with nuclear matter, employing the different assumptions on the nuclear EoS. Fig. 10a shows the equilibrium composition of n-p-e- $\nu_e$ , with the exponent  $\delta$  of the nuclear EoS set at  $\delta = \frac{5}{3}$ . The basic feature of the equilibrium composition is a large electron fraction, imposed by the condition that  $Y_e + Y_{\nu_e} = Y_l$ . The high electron fraction imposes an equal proton fraction, so proto-neutron star matter is much more symmetric at  $\rho \approx \rho_s$  ( $Z/A \approx 0.3$ ) than neutron star matter ( $Z/A \approx 0.1$ ). It is also noteworthy that the neutrino fraction decreases with density (and, correspondingly, the electron fraction increases). This is the result of the equilibrium condition (21), and since  $\mu_n - \mu_p$  rises more rapidly than  $\mu_e - \mu_{\nu_e}$ , the equilibrium is maintained by lowering the neutron fraction. These trends are highly model independent, and similar equilibrium compositions are found for the other values of the exponent  $\delta$ .

Equilibrium compositions of finite temperature matter will always contain some finite population of all particle species, so minute hyperon fractions exist even at  $\rho_s$ . However, these hyperon fractions will build up to significant values only when the potential and kinetic energies of the nucleons make the transition of nucleons to hyperons energetically favorable. Hence, the general features of proto-neutron star matter will be qualitatively similar to those of neutron-star matter discussed above, and significant hyperon formation is expected.

An example for the effects of neutrino trapping and finite temperature on the equilibrium compositions is plotted in Fig. 10b, for the case  $\gamma = \delta = \frac{5}{3}$  and  $-V_{h_1 h_2} = 40$  MeV, for  $Y_l = 0.36$  and a temperature of  $T = 20$  MeV. These compositions appear to be generally similar to those of the corresponding case for neutron star matter (Fig. 3b). Some noticeable differences do still exist, of course: the greater symmetry of the nuclear matter at low densities, imposed by the large electron fraction, reduces the neutron chemical potential with respect to neutron star matter at the same densities. As a result, significant hyperon formation is somewhat delayed in the neutrino trapped matter. The finite temperature slightly enhances this effect, since the nucleon chemical potentials drop below the corresponding value in cold matter. Details relevant to the hyperon formation are as follows:

1. The formation of the negatively charged hyperons is substantially suppressed with respect to that in neutron-star matter, since charge neutrality is handled by the electrons, which must maintain a sizable fraction throughout the entire density range.
2. The formation of the  $\Sigma^-$  gets delayed, and thus the  $\Lambda$  is the most favorable hyperon to be produced at the lower densities. The lack of competition from the  $\Sigma^-$  helps the  $\Lambda$ , precisely as for the neutron star matter case when the  $\Sigma$ 's were excluded by assuming

repulsive  $\Sigma$ -nm interactions. As a result, we find that  $\Lambda$ 's appear first in the matter, at slightly lower densities than when produced in neutron star matter, and it is the  $\Sigma^-$  which comes in a close second. A similar effect governs the fractions of the  $\Sigma^0$ ,  $\Sigma^+$  and  $\Xi^0$  with respect to the  $\Xi^-$ .

3. The total hyperon fraction continues to be smaller than in neutron star matter through the entire density range, although the  $\Lambda$ 's still accumulate to a considerable fraction.
4. The effect of hyperon formation on the lepton population is also worth attention. Once again, the formation of hyperons makes possible the reduction of the neutron fraction without a coupled growth in the proton fraction. Thus the difference  $\mu_n - \mu_p$  decreases, forcing a similar trend in  $\mu_e - \mu_{\nu_e}$ . The immediate result is that hyperon formation is closely followed by a reverse of the trend in the electron and neutrino populations, with respect to those of nuclear matter. The neutrino population begins to rise, and quickly overtakes its value at nuclear saturation density of about 0.06 per baryon, and even crosses 0.1 per baryon at high densities.

Again, the results found here with the effective EoS bear high resemblance to those reported in works which used more sophisticated models [9].

The above results depend only little on temperature, and similar equilibrium compositions are found for any significant temperature ( $T \geq 10$  MeV). The temperature determines the precise hyperon populations at low densities, but these are insignificantly low anyway. There is some model dependence with respect to the parameterization of the baryon-baryon effective interaction (the values of  $\gamma$  and  $\delta$ ), in a similar fashion as for neutron star matter. Again, very little dependence is found regarding the value of the hyperon-hyperon well depth, which is of even less importance in the present case, as the matter is even more nucleon dominated.

Similar results are found for the case of a repulsive  $\Sigma$ -nm interaction, excluding  $\Sigma$ 's from the matter. The equilibrium compositions for proto-neutron-star matter with  $\gamma = \delta = \frac{5}{3}$  and  $-V_{h_1h_2} = 40$  MeV, but when the  $\Sigma$ 's are excluded, are plotted in Fig. 10c. Since the formation of the  $\Sigma^-$  is suppressed even when allowed,  $\Lambda$ 's dominate inherently and the  $\Lambda$  fraction is rather insensitive to the presence of  $\Sigma$ 's. Excluding them does create an increase, obviously, in the  $\Xi$  fraction.

The outstanding point of proto-neutron star composition is that it generates a different equation of state than for neutron star (neutrino-free) matter. In nuclear matter the effect is trivial: the greater symmetry among the nucleons lowers the total Fermi energies and the symmetry potential energy density. Hence, equilibrium nuclear matter with trapped neutrinos is inherently softer than neutrino-free nuclear matter for the same nuclear-force model.

The picture is quite the opposite when hyperons enter the game. As discussed above, the more symmetric nuclear fraction somewhat suppresses hyperon formation in neutrino-trapped matter. Since hyperon formation imposes a softer equation of state by lowering kinetic and potential energies, it is clear that when hyperons are allowed to appear the equation of state for neutrino-trapped matter, which has a smaller hyperon fraction will be stiffer than the EoS for neutrino free matter. This principle was pointed out in [7,8], and is laid out in detail in [9]. The equations of state calculated here do indeed reproduce these expected results. Fig. 11 compares pressure vs. baryon density (which is the relevant quantity when using the same model for different thermodynamic conditions), for  $\delta=\gamma=\frac{5}{3}$  and  $-V_{h_1 h_2}=40$  MeV. As is expected for nuclear matter (Fig. 11a) the neutrino-trapped case (dashed line) is clearly softer (except at very low densities, where the finite-temperature lepton pressure is of significance). Matter with hyperons presents the opposite state of affairs (Figs. 11b and 11c): as is clearly seen, the neutrino-trapped cases do indeed have stiffer equations of state than the neutrino-free ones (solid lines).

## 6 Results: Respective Neutron Star Masses

A natural test for the constructed equations of state is the calculation of the neutron star properties they predict. Most important of these is, of course, the mass/centeral-density relation: the mass sequence  $M(\varepsilon_c)$ , of the neutron star for a given equation of state, and especially the maximum mass predicted by the equation. This maximum mass must be at least  $1.4 M_\odot$ , which is the well determined observed mass of the Hulse-Taylor pulsar (see [36] for a recent review of observed and calculated neutron star properties), where  $M_\odot \equiv 1.989 \times 10^{33}$  gm is the standard notation for one solar mass.

In this study we limit our discussion to calculating the static neutron star masses, noting that rotation may add as much as 0.1-0.2  $M_\odot$  [36]. The static masses are calculated by numerical integration of the Tolman-Oppenheimer-Volkoff equations [37] of hydrostatical equilibrium, namely (setting  $G=c=1$ , so that all physical quantities are given in centimeters,  $M_\odot \equiv 1.477 \times 10^5$  cm):

$$\frac{dm}{dr} = 4\pi r^2 \varepsilon \quad ; \quad \frac{dP}{dr} = -\frac{\varepsilon m}{r^2} \left(1 + \frac{P}{\varepsilon}\right) \left(1 + \frac{4\pi r^3 P}{m}\right) \left(1 - \frac{2m}{r}\right)^{-1} \quad (32)$$

(and  $\frac{d\Phi}{dr} = \frac{1}{\varepsilon} \frac{dP}{dr} \left(1 + \frac{P}{\varepsilon}\right)^{-1}$  for the field  $\Phi$ ) .

These equations are solved following the recipe of Arnett and Bowers [38], by setting a central density  $\varepsilon_c$  in the star and integrating outwards until reaching zero pressure. The equation of

state of Baym, Pethick and Sutherland [39] is used for the subnuclear densities. The specific choice of the EoS for these densities is actually unimportant for the mass sequence, as the fraction of the neutron star mass originating from the subnuclear densities is insignificant.

## 6.1 Neutron Star Masses

The predicted mass sequences for the three equations of state for nuclear matter ( $\delta = 2, \frac{5}{3}$  and  $\frac{4}{3}$ ) are plotted in Fig. 12 as a function of the central density. As is expected from the large difference between these equations (Fig. 6), the neutron star mass sequences vary considerably from one equation to another. For the stiffest equation ( $\delta = 2$ ), at  $\varepsilon_c = 1.25 \times 10^{15}$  gm/cm<sup>3</sup>, after which the EoS breaks causality, the mass begins to saturate at the very high value of  $2.6 M_\odot$ . The softest equation, which is still stiff in comparison to most of the more sophisticated nuclear matter models, yields a maximum mass of about  $2.2 M_\odot$ .

The consequences of the relative similarities between the equations of state for matter with hyperons are even enhanced in the neutron star mass calculations. As noted in Section 5, the dominant factor for the EoS is the number of species that are available for production in the matter, the case of a repulsive  $\Sigma$ -nm interaction being clearly different than the attractive one, and both are very different than the nuclear matter EoS.

Fig. 13 presents six plots of neutron star mass sequences. In all cases the hyperon-hyperon well depth is chosen as  $-V_{h_1 h_2} = 40$  MeV, and the curves differ in the short range repulsive forces model, i.e. in the values of  $\gamma$  and  $\delta$ . For comparison, the mass function of the softest nuclear matter equation  $\delta = \frac{4}{3}$  is also plotted. The outstanding result is that while in each case the masses corresponding to low densities are very model dependent in terms of the short range interactions (the values of  $\gamma$  and  $\delta$ ), the maximum masses are very similar for different equations of the same type (including or excluding the  $\Sigma$ 's). The behavior at low central densities must be different, as it results mainly from the nucleon-nucleon interactions, which determine the precise model dependence. The similarity of the mass sequences at high central densities is a direct consequence of the hyperon "pressure control" mechanism, discussed in the previous Section. This mechanism is basically dependent only on the availability of the various hyperon species for formation in the matter - and hence, the clear distinction between matter which may contain  $\Sigma$ 's and matter which does not.

*These results clearly indicate that the appearance of hyperons makes the maximum mass of neutron stars sensitive only to the gross properties of the baryon-baryon interactions, and almost insensitive to specific details. While these results generated with effective equations of state can hardly be considered as proof of such a trend, we do believe that they do serve as indication that it is the number of available species that dominates the neutron star mass*

function at high density.

The precise values of the resulting maximum masses are also of interest. Since the baryonic matter EoS is softer than that for nuclear matter, the maximum neutron star masses are expectedly smaller. The maximum mass in the various models for matter without  $\Sigma$ 's are about  $1.6\text{--}1.7 M_\odot$ , while the softer matter with  $\Sigma$ 's holds maximal masses of only about  $1.4\text{--}1.5 M_\odot$ . The proximity of the latter value to the upper limit of observed neutron star masses ( $1.44 M_\odot$  of PSR 1913+16) may be viewed in two ways: as an indication that  $\Sigma$ 's are bound in the matter, thus limiting the maximal mass to less than  $1.5 M_\odot$ ; or on the contrary - since the EoS with  $\Sigma$ 's yields such a border-line result, then perhaps it is more plausible that  $\Sigma$ 's are unbound in the matter. This possibility is enhanced by the recent suggestions that the mass of the Vela Pulsar is above  $1.55 M_\odot$ , based on analysis of its X-ray source properties [40].

While we are unaware of an explicit indication to a hyperon induced “pressure control” mechanism in previous works, it is interesting to note that most studies which include hyperons in neutron star matter find that the maximum masses lie within a narrow range, typically  $1.4\text{--}1.7 M_\odot$  (see Refs. [1, 3, 4, 10, 36, 38] and other references therein), not unlike the results presented here. On the other hand, published neutron star maximum masses for nuclear equations of state do indeed vary over a larger range ( $1.5\text{--}2.5 M_\odot$ ), and are usually larger than  $1.8 M_\odot$  [ibid.]. Both these results are consistent with the hyperon induced “pressure control” mechanism discussed above.

We complete this study by remarking that all results show little dependence on the hyperon-hyperon well depth, as is expected for nucleon-dominated matter. Choosing a large well depth along with a steep high density repulsion ( $\gamma = 2$ ) creates greater repulsion at high densities, leading to a stiffer EoS and a slightly higher maximal mass. However, we find that this effect changes the maximum mass by  $\Delta M \leq 0.1 M_\odot$  between the case of strong hyperon-hyperon interactions and the case when these interactions are turned off.

## 6.2 Proto Neutron Star Masses

Realistic proto-neutron star calculations require consistent thermodynamic solutions, in order to establish the physical temperature profile for the star (as the star's physical state is probably closer to constant entropy per baryon rather than constant temperature). We thus limit ourselves to simplified static solutions, in order to recover the key feature of proto-neutron star masses.

Since the EoS for nuclear matter stiffens when neutrinos diffuse out of the proto-neutron

star, the maximal mass of the fully evolved neutron star will be greater than that of the proto-neutron star. Hence, if a stable proto-neutron star is formed in the supernova (and does not collapse initially into a black hole), it will also have a stable configuration in the fully evolved state.

The opposite trend in matter with hyperons also brings about the possibility of the reverse physical scenario: since the equation of state for matter with hyperons softens as the neutrinos diffuse outward (and the hyperon population increases), the maximal mass of the proto-neutron star will be greater than that of the fully evolved star, under the same physical assumptions. Thus, the stage is set for a delayed collapse of the proto-neutron star into a black hole, if its mass will be too large for the neutrino-free equation of state. Such a scenario has been motivated by the combination of a neutrino pulse in SN1987A (so there was no initial collapse into a black hole), and the fact that no pulsar has been detected; see Refs. [7-10].

We reproduced the necessary features described above in the effective EoS scheme, when deriving mass sequences for proto-neutron stars and evolved neutron stars (Fig. 11). For nuclear matter the EoS for proto-neutron star (neutrino-trapped) is softer than for evolved neutron star (neutrino-free) and the maximal mass drops from  $\sim 2.4 M_{\odot}$  to  $\sim 2.0 M_{\odot}$  for the proto-neutron star. Since the EoS for neutrino-trapped matter is stiffer for matter with hyperons, the maximal mass of the proto-neutron star is found to be larger for the hyperonic case. For matter with all types of hyperons the maximum mass of the proto-neutron star is almost  $1.7 M_{\odot}$  (with respect to a little over  $1.4 M_{\odot}$  for the evolved neutron star). Matter with no  $\Sigma$ 's is less affected by the neutrino diffusion (as explained above, the  $\Sigma$ 's are somewhat suppressed in neutrino-trapped matter) but the proto-neutron star still has a maximum mass of about  $0.1 M_{\odot}$  higher than that of the evolved star ( $1.8 M_{\odot}$  vs.  $1.7 M_{\odot}$ ). This trend appears for the other various cases of assumptions made about the baryon-baryon interaction and shows only little model dependence, as in the case of the evolved neutron star masses.

## 7 Conclusions and Discussion

The effective equation of state described in the present study is designed to allow rapid calculations and extensive parameter surveys of high density matter rich with strange baryons. This equation generalizes the Lattimer-Swesty EoS for nuclear matter, and is constructed so that it will reproduce the physical features attributed to such matter, while not presuming to correctly describe the microscopic details of the underlying physics. Its construction is performed by basing the EoS on local (effective) potentials for the various components of

the baryon-baryon interaction, which are constrained as much as possible by experimental data from hypernuclei.

In view of the large uncertainties in the baryon-baryon interactions, especially at high densities, we examine the properties of the EoS with various assumptions regarding these interactions. We investigate sensitivity to the density dependence of the repulsive term and remark on the unknown power of the hyperon-hyperon interactions. Special attention is given to the consequences of a recent analysis of  $\Sigma$ -atoms data, which suggests a strong isoscalar repulsion in the  $\Sigma$ -nuclear matter ( $\Sigma$ -nm) interaction (very different than the commonly assumed interaction), and excludes  $\Sigma$  hyperons from forming in the high density matter.

We find that the effective equation of state yields similar equilibrium compositions and equations of state as found in equivalent RMF models. The main features of the hyperon formation in zero-temperature neutrino free matter (typical of evolved neutron star interiors) are:

1. Hyperons begin to appear in the matter at about twice the nuclear saturation density  $\rho_s \approx 0.155 \text{ fm}^{-3}$ , and at  $2.5\rho_s$  the hyperon fraction in the matter is already significant. First to appear are the  $\Sigma^-$  (due to its negative charge) and the  $\Lambda$ , or the  $\Lambda$  alone, depending on the assumed  $\Sigma$ -nm interaction. Other hyperons follow at higher densities.
2. Hyperon production is followed by considerable deleptonization, as negatively charged hyperons replace electrons and muons in maintaining charge neutrality.

We find that these features are typical of all models, although the details are model-dependent as far as the density dependence of the baryon-baryon repulsive interaction terms. Since the matter is dominated by nucleons in most of the density range in question, there is little dependence on the hyperon-hyperon interactions.

The key effect of the appearance of hyperons in the matter is the softening of the equation of state, due to the lowering of both repulsion and Fermi energies as the total baryon density is divided among a larger number of species. We emphasize that *hyperons serve as a “pressure control” mechanism in the high density matter*, since the extent of their appearance is directly related to the details of the nuclear interactions. Thus, while for nuclear matter a more powerful nucleon-nucleon repulsion creates a stiffer EoS, in baryonic matter an enhanced production of hyperons will occur, restoring the gross properties of the EoS. The immediate result of this “pressure control” by the hyperons is that all EoS including hyperons are very similar, the only significant model dependence being on the number of available species (i.e. the general features of the  $\Sigma$ -nm interaction discussed above).

The most notable manifestation of this effect is in the predicted maximum masses of neutron stars. By solving the static mass functions of neutron stars for the various equations, we find that the hyperon-imposed similarity in the equations of state leads to very moderate specific-model-dependence of the maximum masses. *While the maximum mass for nuclear matter is highly model dependent, the maximum masses for matter with hyperons depend almost entirely just on the number of available species.* Specifically, we find that for matter which includes  $\Sigma$ 's, the maximum mass for all equations of state are about  $1.4\text{--}1.5 M_{\odot}$ , while for the case of excluded  $\Sigma$ 's, maximum masses are all in the range  $1.6\text{--}1.7 M_{\odot}$ . Such analysis with an effective equation of state may hardly be considered as a proof of this point, but we do believe that the general trend described above indicates a genuine physical principle.

It is interesting that the result for matter with  $\Sigma$ 's yields just about the maximum observed neutron star mass (the small difference can be bridged by allowing also for rotation and finite temperature). This may be viewed in two ways: one could either argue that this is too border-line a result, implying  $\Sigma$ 's should be excluded, or rather find this an indication that the maximum mass is indeed close to the observed value, as determined by the hyperons. Clearly further analysis is needed to elaborate on this point.

We briefly investigate the properties of proto-neutron star matter, which has a finite temperature and in which neutrinos are assumed to be trapped, so that the total lepton number remains constant. Such matter is relevant to the simulation of proto-neutron star evolution and core-collapse process in supernovae. Again we find that hyperons appear at about  $2\rho_s$  and accumulate significantly by  $2.5\rho_s$ , with very weak model dependence. Hyperon appearance changes the trend of the neutrino population, which begins to increase rather than decrease at higher densities, since the hyperons indirectly lower the electron fraction required to maintain charge neutrality. These results are in good agreement with studies performed with more sophisticated models.

The formation of hyperons softens the equation of state for core-collapse matter as well, and once again serves as “pressure control” for the nucleons. The softening occurs, of course, at the density of hyperon accumulation, which is border-line with regard to the densities reached during the supernova. None the less, a softer equation of state is appealing, as it will strengthen the shock and the neutrino delayed shock, thus strengthening the explosion. In the proto-neutron star case such a softening is clearly important, and we do reproduce the well-known tendency of the maximum mass for matter with trapped neutrinos being larger than that for neutrino free matter. This feature, which is typical for matter with hyperons and opposite to the one prevalent in nuclear matter, opens the way for the “delayed collapse” scenario, motivated by the lack of an observed pulsar in the Supernova 1987A remnant. In such a scenario, a newly formed neutron star could exist in a meta-stable configuration,

collapsing into a black hole when the neutrinos diffuse out of the star leaving it with too large a mass.

All of the above results serve as indication that the effective equation of state may be treated as a trustworthy tool in the analysis of high density matter with strangeness. Nonetheless, some further extension of the equation should be considered. One area for improvement is the description of the high density behavior of the forces. A possible approach would be to add another repulsive term  $c'\rho^{\gamma'}$ , where  $\gamma'$  will be greater than  $\gamma$  (which could then be set to a low value allowing consistently for a low nuclear incompressibility). This new repulsive term could be set universally for all species (e.g, if it may be attributed to quark degrees of freedom). This is somewhat similar to a suggestion by Lattimer, Swesty and Myra [24], that the repulsive term in the energy density formula be amended to  $c\rho^{\delta+1}/(1+d\rho^{\delta-1})$ , as an ad hoc method to artificially soften the equation.

Other possible improvements are introducing finite ranges to the forces, and a more comprehensive treatment of effective masses. Clearly, any future experimental and theoretical constraints on the nuclear, nucleon-hyperon and hyperon-hyperon forces must be incorporated into the equation and its parameters as well.

Introduction of  $\pi$  and  $K$  condensates should also be considered, although viewed as unlikely by several current works. The same applies to the formation of  $\Delta$  isobars, which are found to be excluded from the matter by using standard assumptions regarding its interactions and mass. A natural extension of the equation would be to include a deconfined quark phase at high densities, for which an effective equation of state is quite simple [23].

Further work is also required regarding the implications of strangeness on high density matter in astrophysical contexts. Up to date no neutron star property that can be uniquely connected to hyperon formation has been suggested, although observed cooling rates have been shown to place some limits on the matter composition (a large hyperon fraction along with a significant lepton population would produce much too large cooling rates through the direct Urca mechanism). Studies of possible implications of hyperon formation on rotational properties of neutron stars, along with magnetic, superconducting and superfluid behavior of such matter, and crust properties with relation to observed glitches should also be considered (far more extensive studies on these subjects have been carried out for strange-quark-stars, following the still debated stable-strange-matter hypothesis). We note that a recent work by Glendenning, Pei and Weber [41] suggests that the existence of a quark-matter core (which will definitely include a non-zero-strangeness-fraction) could be identified by its effect on the pulsar breaking index, if such a core builds up during the pulsar spin down.

A unique signature of hyperon (and generally strange particles) production in proto-neutron

star would also be of considerable interest, especially regarding the “delayed-collapse” scenario and whether it may lead to an appreciable effect on the neutrino pulse from the proto-neutron star [8]. Studies along these lines have begun in recent years, and are well worth continuing.

Last but clearly not least, the results presented in this study imply that hyperon formation may be of importance in core-collapse supernovae, if densities equal or greater to twice the nuclear saturation density are reached in the collapsing core prior to the “bounce”. A softened equation of state might claim its role in the shock-wave/neutrino-delayed-shock process, presumably strengthening the explosion.

We are grateful to Sidney Kahana for stimulating discussions about high density matter and baryon-baryon interactions. We further wish to thank Eliahu Friedman, Itamar Lichtenstadt, Greg Cook and Nir Barnea for helpful suggestions and advice during the preparation of this manuscript. This research was supported in part by the U.S-Israel Binational Science Foundation.

## References

- [1] V.R. Pandahripande, Nucl. Phys. A178 (1971) 123.
- [2] H.A. Bethe and M.B. Johnson, Nucl. Phys. A230 (1974) 1.
- [3] N.K. Glendenning, Ap. J. 293 (1985) 470.
- [4] P.J. Ellis, R. Knorren and M. Prakash, Phys. Lett. B349 (1995) 11; R. Knorren, M. Prakash and P.J. Ellis, Phys. Rev. C52 (1995) 3470.
- [5] J. Schaffner and I.N. Mishustin, Phys. Rev. C53 (1996) 1416.
- [6] R.W. Mayle, M. Tavani and J.R. Wilson, Ap. J. 418 (1993) 398.
- [7] W. Kiel and H.T. Janka, Astron. and Astrophys. 296 (1995) 145.
- [8] H.A. Bethe and G.E. Brown, Ap. J. 423 (1994) 659.
- [9] M. Prakash, I. Bombaci, M. Prakash, P.J. Ellis, J.M. Lattimer and R. Knorren, Phys. Rep. 280 (1997) 1.
- [10] P.J. Ellis, J.M. Lattimer and M. Prakash, Com. Nucl. Part. Phys. 22 (1996) 63.
- [11] J.M. Lattimer and F.D. Swesty, Nucl. Phys. A535 (1991) 331 [LS].
- [12] E. Baron, J. Cooperstein and S. Kahana, Nucl. Phys. A440 (1985) 744.
- [13] C.J. Batty, E. Friedman and A. Gal, Phys. Lett. 335 (1994) 273; Prog. Theo. Phys. Suppl. 117 (1994) 145.
- [14] J. Mares, E. Friedman, A. Gal and B.K. Jennings, Nucl. Phys. A594 (1995) 311.
- [15] J.M. Lattimer, C.J. Pethick, D.G. Ravenhall and D.Q. Lamb, Nucl.Phys. A432 (1985) 646.
- [16] D. Vautherin, in: Supernovae, S. Bludman, R. Mochkovitch and J. Zinn-Justin eds., (Elsevier Science, 1994), p. 345.
- [17] D.J. Millener, C.B. Dover, and A. Gal, Phys. Rev. C38 (1988) 2700 [MDG].
- [18] H.A. Bethe, Rev. Mod. Phys. 62 (1990) 801.
- [19] A. Burrows, Ap. J. 334 (1988) 891.

- [20] F. Weber and M.K. Weigel, Nucl. Phys. A505, (1989) 779.
- [21] G.E. Brown, K. Kubodera, M. Rho and V. Thorsson, Phys. Lett. B291 (1992) 355; G.E. Brown, C-H. Lee, M. Rho and V. Thorsson, Nucl. Phys. A567 (1994) 937; V. Thorsson, M. Prakash and J.M. Lattimer, Nucl. Phys. A572 (1994) 693; G.Q. Li, H.C. Lee and G.E. Brown, Nucl. Phys. A (in this volume, 1997).
- [22] J. Schaffner, A. Gal, I. Mishustin, H. Stocker and W. Greiner, Phys. Lett. B324 (1994) 268.
- [23] C.R. Alcock, E. Farhi and A. Olinto, Ap. J. 310 (1986) 261.
- [24] F.D. Swesty, J.M. Lattimer and E.S. Myra, Ap. J. 425 (1994) 195.
- [25] R.E. Chrien and C.B. Dover, Ann. Rev. Nuc. Part. Sci. 39 (1989) 227.
- [26] C.B. Dover and A. Gal, Prog. Nucl. Phys., D. Wilkinson ed. (Pergamon Press, Oxford, 1984), vol. 12, p. 171.
- [27] C.B. Dover and A. Gal, Ann. Phys. 146 (1983) 209.
- [28] J. Schaffner, C.B. Dover, A. Gal, C. Greiner, D.J. Millener and H. Stocker, Ann. Phys. 235 (1994) 35.
- [29] A.R. Bodmer and Q.N. Usmani, Nucl. Phys. A468 (1987) 653.
- [30] J. Schaffner-Bielich, I.N. Mishustin and J. Bondorf, Nucl. Phys. A (in this volume, 1997).
- [31] M. Barranco and J. Treiner, Nucl. Phys. A351 (1981) 269.
- [32] C.J. Pethick, Rev. Mod. Phys. 64 (1992) 1133.
- [33] M. Prakash, M. Prakash, J.M. Lattimer and C.J. Pethick, Ap. J. 390 (1992) L77.
- [34] M. Prakash, Phys. Rep. 242 (1994) 297.
- [35] C. Shaab, F. Weber, M.K. Weigel and N.K. Glendenning, Nuc. Phys. A605 (1996) 531.
- [36] G.B. Cook, S.L. Shapiro and S.A. Teukolsky, Ap. J. 424 (1994) 823.
- [37] R.C. Tolman, Proc. Nat. Acad. Sci. USA 20 (1934) 3; J.R. Oppenheimer and G.M. Volkoff, Phys. Rev. 55 (1939) 374.
- [38] W.D. Arnett and R.L. Bowers, Ap. J. Suppl. 33 (1977) 415.

- [39] G. Baym, C.J. Pethick and P. Sutherland, Ap. J. 170 (1971) 299.
- [40] F.Nagase, Proc. Astr. Soc. Jap. 41 (1989), 1; M.H. van Kerkwijk, J. van Paradijs, E.J. Zuiderwijk, G. Hammerschlag-Hensberge, L. Kaper and C. Sterken, Astron. and Astrophys. 303 (1995) 483.
- [41] N.K. Glendenning, S. Pei and F. Weber, LBL report LBL-39746 (1997).

## Figure Captions

Fig. 1. The density dependence of  $\Lambda$  potential in nuclear matter,  $V_{\Lambda N}(\rho_N) = a_{\Lambda N}\rho_N + c_{\Lambda N}\rho_N^\gamma$ , for different values of the exponent  $\gamma$  in the repulsion term, using the parametrs sets of MDG [17] given in Table 2. The arrow marks the nuclear saturation density,  $\rho_s = 0.155 \text{ fm}^{-3}$ .

Fig. 2. The equilibrium compositions of nuclear matter (n-p-e- $\mu$ ) as a function of baryon density for the case  $\delta = 2$ ; see Eq. (5) and Table 1. Other models of the nuclear interaction (different values of  $\delta$ ) yield similar equilibrium compositions.

Fig. 3a. The equilibrium compositions for matter containing hyperons as well as nucleons and leptons, for  $\delta = \gamma = 2$  (see Eq. (6)), and for the hyperon-hyperon well depth  $-V_{h_1 h_2} = 40 \text{ MeV}$ .

Fig. 3b. Same as 3a but with  $\delta = \gamma = \frac{5}{3}$ .

Fig. 3c. Same as 3a but with  $\delta = \gamma = \frac{4}{3}$ .

Fig. 4a. The equilibrium compositions for matter containing  $\Lambda$ 's and  $\Xi$ 's as well as nucleons and leptons, but no  $\Sigma$ 's (when a repulsive  $\Sigma$ -nm interaction is assumed), for  $\delta = \gamma = 2$ , and a hyperon-hyperon well depth  $-V_{h_1 h_2} = 40 \text{ MeV}$ .

Fig. 4b. Same as 4a but with  $\delta = \gamma = \frac{5}{3}$ .

Fig. 4c. Same as 4a but with  $\delta = \gamma = \frac{4}{3}$ .

Fig. 5. Same as 3a but with hyperon-hyperon interactions “turned off”.

Fig. 6. Equations of state for nuclear matter (n-p-e- $\mu$ ) for the different models of the nucleon potential energy density. The equations for  $\delta = 2$  and  $\frac{5}{3}$  break causality at  $1.25 \times 10^{15} \text{ gm/cm}^3$  and  $1.94 \times 10^{15} \text{ gm/cm}^3$ , respectively, as indicated by the dashed curves.

Fig. 7. Equations of state for high density matter with nucleons and leptons alone; nucleons, hyperons and leptons; and  $\Lambda$ 's and  $\Xi$ 's as well as nucleons and leptons, but no  $\Sigma$ 's (for a repulsive  $\Sigma$ -nm interaction). The parameters used are  $\delta = \gamma = \frac{5}{3}$ , and  $-V_{h_1 h_2} = 40 \text{ MeV}$ .

Fig. 8. Equations of state for high density matter with nucleons, hyperons (assuming an attractive  $\Sigma$ -nm interaction) and leptons, for different choices of the baryon potential energy density dependence,  $\delta = \gamma = 2, \frac{5}{3}$  and  $\frac{4}{3}$ , and a hyperon-hyperon well depth  $-V_{h_1 h_2} = 40 \text{ MeV}$ . The equations of state correspond to the equilibrium compositions of Figs. 3a, 3b and 3c.

Fig. 9. The effect of hyperon formation on the adiabatic index  $\Gamma$  of the EoS for the case of  $\delta = \gamma = \frac{5}{3}$ , and  $-V_{h_1 h_2} = 40 \text{ MeV}$ , compared to the corresponding EoS for nuclear matter. Each “dip” in the curve of the adiabatic index corresponds to the appearance of a new hyperon species.

Fig. 10a. The equilibrium compositions of neutrino trapped nuclear matter (n-p-e- $\nu_e$ ) as a function of baryon density for the case  $\delta = \frac{5}{3}$ , with a lepton fraction of  $Y_l = 0.36$  and temperature  $T = 20$  MeV. The equilibrium compositions for other models of the nuclear interaction (values of  $\delta$ ) are very similar.

Fig. 10b. The equilibrium compositions for neutrino-trapped matter containing hyperons as well as nucleons and leptons, where  $\delta = \gamma = \frac{5}{3}$ , and  $-V_{h_1 h_2} = 40$  MeV.

Fig. 10c. The equilibrium compositions for neutrino-trapped matter containing hyperons as well as nucleons and leptons, but no  $\Sigma$ 's (for a repulsive  $\Sigma$ -nm interaction), for  $\delta = \gamma = \frac{5}{3}$  and  $-V_{h_1 h_2} = 40$  MeV.

Fig. 11. Equations of state for neutrino-free matter (solid lines) and neutrino-trapped matter (dashed lines) for  $\delta = \gamma = \frac{5}{3}$ , for the different versions of high density matter: nucleons only (a), nucleons and all hyperons (b) and nucleons,  $\Lambda$ 's and  $\Xi$ 's but no  $\Sigma$ 's (c). It is noticeable that the EoS for the neutrino-trapped case is softer for nuclear matter, but stiffer for matter with hyperons.

Fig. 12. Neutron star mass vs. central density mass-sequences for nuclear matter (n-p-e- $\mu$ ) for the different models of the nucleon potential energy density.

Fig. 13. Neutron stars mass vs. central density mass-sequences for high density matter with all hyperon species and with only  $\Lambda$ 's and  $\Xi$ 's but no  $\Sigma$ 's (for a repulsive  $\Sigma$ -nm interaction), for different values of  $\gamma$  and  $\delta$ . In all cases the hyperon-hyperon well depth is  $-V_{h_1 h_2} = 40$  MeV. Also plotted is the neutron star mass sequence for the softest equation for nuclear matter  $\delta = \frac{4}{3}$ .

Table 1:

Values for the parameters of the terms corresponding to the nuclear potential energy density of Eq. (5), as derived from the Lattimer-Swesty equation of state with  $m^* = m$ .

$\delta$	$a_{NN}$ [MeV fm <sup>3</sup> ]	$b_{NN}$ [MeV fm <sup>3</sup> ]	$c_{NN}$ [MeV fm <sup>3<math>\delta</math></sup> ]
2	-784.4	214.2	1936.0
$\frac{5}{3}$	-935.4	214.2	1557.2
$\frac{4}{3}$	-1384.6	214.2	1672.8

Table 2:

Values for the parameters of the terms corresponding to the  $\Lambda$ -nm interactions in the local potential energy model of Eq. (6), for a well-depth of  $-V_{\Lambda N} = 28$  MeV at nuclear saturation density.

$\gamma$	$a_{\Lambda N}$ [MeV fm <sup>3</sup> ]	$c_{\Lambda N}$ [MeV fm <sup>3<math>\gamma</math></sup> ]
2	-340.0	1087.5
$\frac{5}{3}$	-387.0	738.8
$\frac{4}{3}$	-505.2	605.5

Table 3:

Values for the parameters of the terms corresponding to the  $\Sigma$ -nm interactions in the local potential energy model of Eq. (6), for a well-depth of  $-V_{\Sigma N} = 28$  MeV at nuclear saturation density, assuming a  $\Sigma$ -nm interaction equal to the  $\Lambda$ -nm one, except for a nonzero isovector term twice that of the N-nm interaction.

$\gamma$	$a_{\Sigma N}$ [MeV fm <sup>3</sup> ]	$b_{\Sigma N}$ [MeV fm <sup>3</sup> ]	$c_{\Sigma N}$ [MeV fm <sup>3\gamma</sup> ]
2	-340.0	214.2	1087.5
$\frac{5}{3}$	-387.0	214.2	738.8
$\frac{4}{3}$	-505.2	214.2	605.5

Table 4:

Values for the parameters of the terms corresponding to the  $\Sigma$ -nm interactions in the local potential energy model of Eq. (29), accepting the strong  $\Sigma$ -nm isoscalar repulsion argued for in Ref. [13]. The  $b$  and  $B$  parameters are given in fm.

$\alpha$	$b_0$	$B_0$	$b_1$	$B_1$
0.5	2.1	-4.3	-1.0	0

Table 5:

Values for the parameters of the terms corresponding to the  $\Xi$ -nm interactions in the local potential energy model of Eq. (6), for a well-depth of  $-V_{\Xi N} = 24$  MeV at nuclear saturation density.

$\gamma$	$a_{\Xi N}$ [MeV fm <sup>3</sup> ]	$b_{\Xi N}$ [MeV fm <sup>3</sup> ]	$c_{\Xi N}$ [MeV fm <sup>3\gamma</sup> ]
2	-291.5	0	932.5
$\frac{5}{3}$	-331.8	0	663.4
$\frac{4}{3}$	-434.4	0	520.1

Table 6:

Values for the parameters of the terms corresponding to the various hyperon-hyperon interactions in the local potential energy model of Eq. (6), assuming the hyperon-hyperon well-depth at a density equal to the nuclear saturation density to be  $-V_{h_1 h_2} = 40$  MeV. Only the  $\Sigma$ 's are assumed to have a nonzero isovector component in their interactions.

$\gamma$	$a_{YY}$ [MeV fm <sup>3</sup> ]	$b_{\Lambda Y} = b_{\Xi Y}$ [MeV fm <sup>3</sup> ]	$b_{\Sigma\Sigma}$ [MeV fm <sup>3</sup> ]	$c_{YY}$ [MeV fm <sup>3</sup> γ]
2	-486.2	0	428.4	1553.6
$\frac{5}{3}$	-552.6	0	428.4	1055.4
$\frac{4}{3}$	-723.2	0	428.4	869.0

figure 1

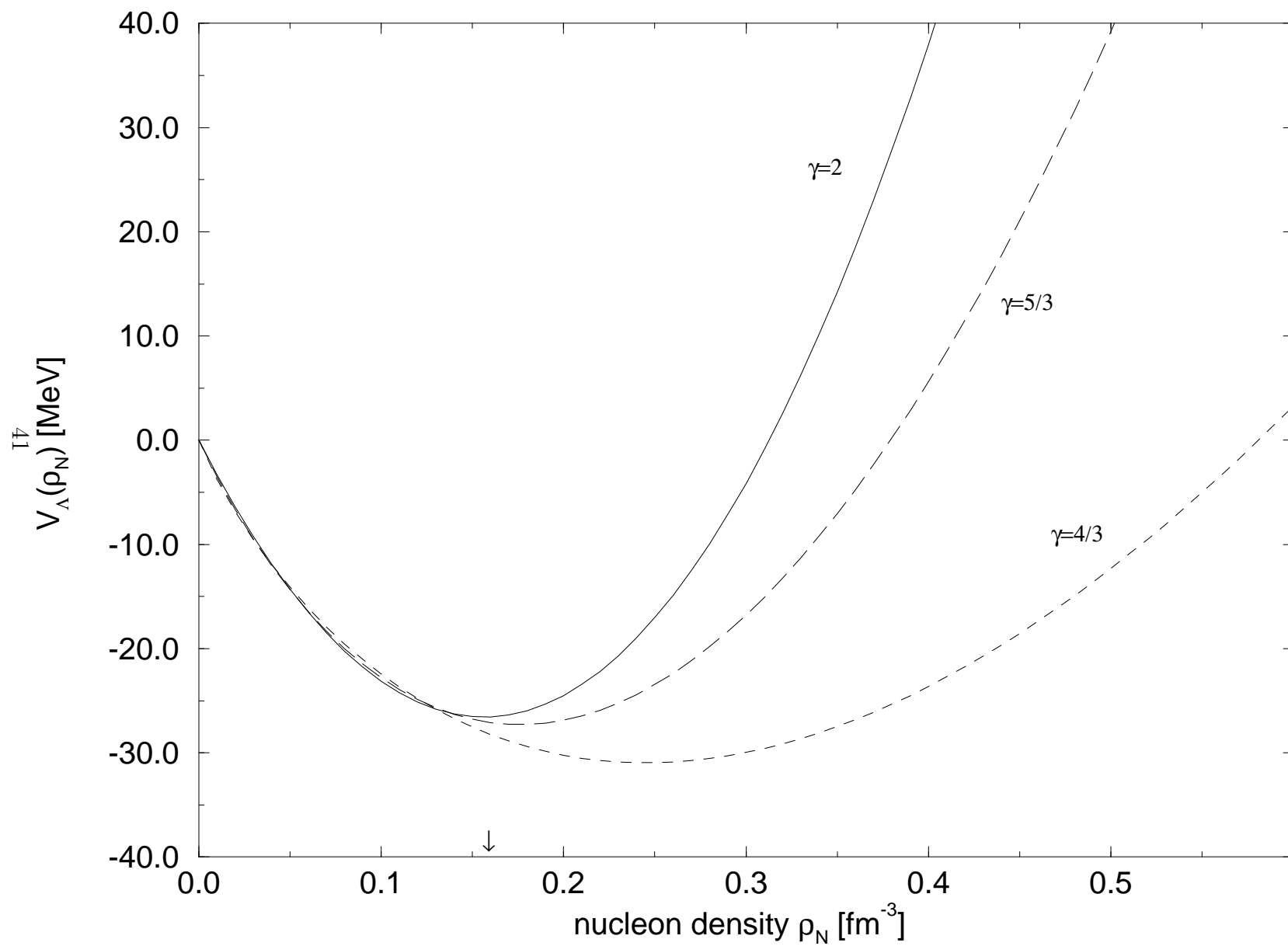


figure 2

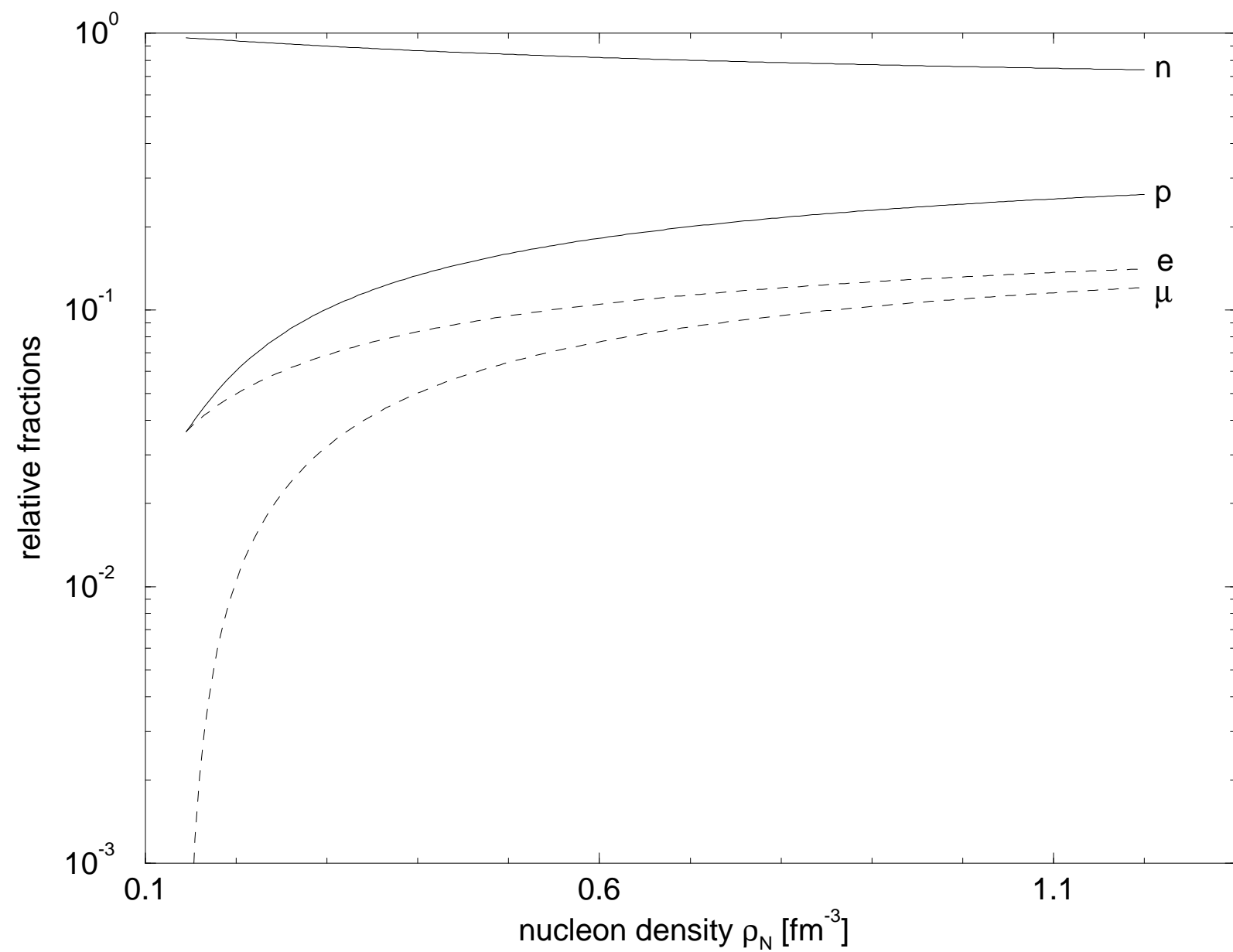


figure 3

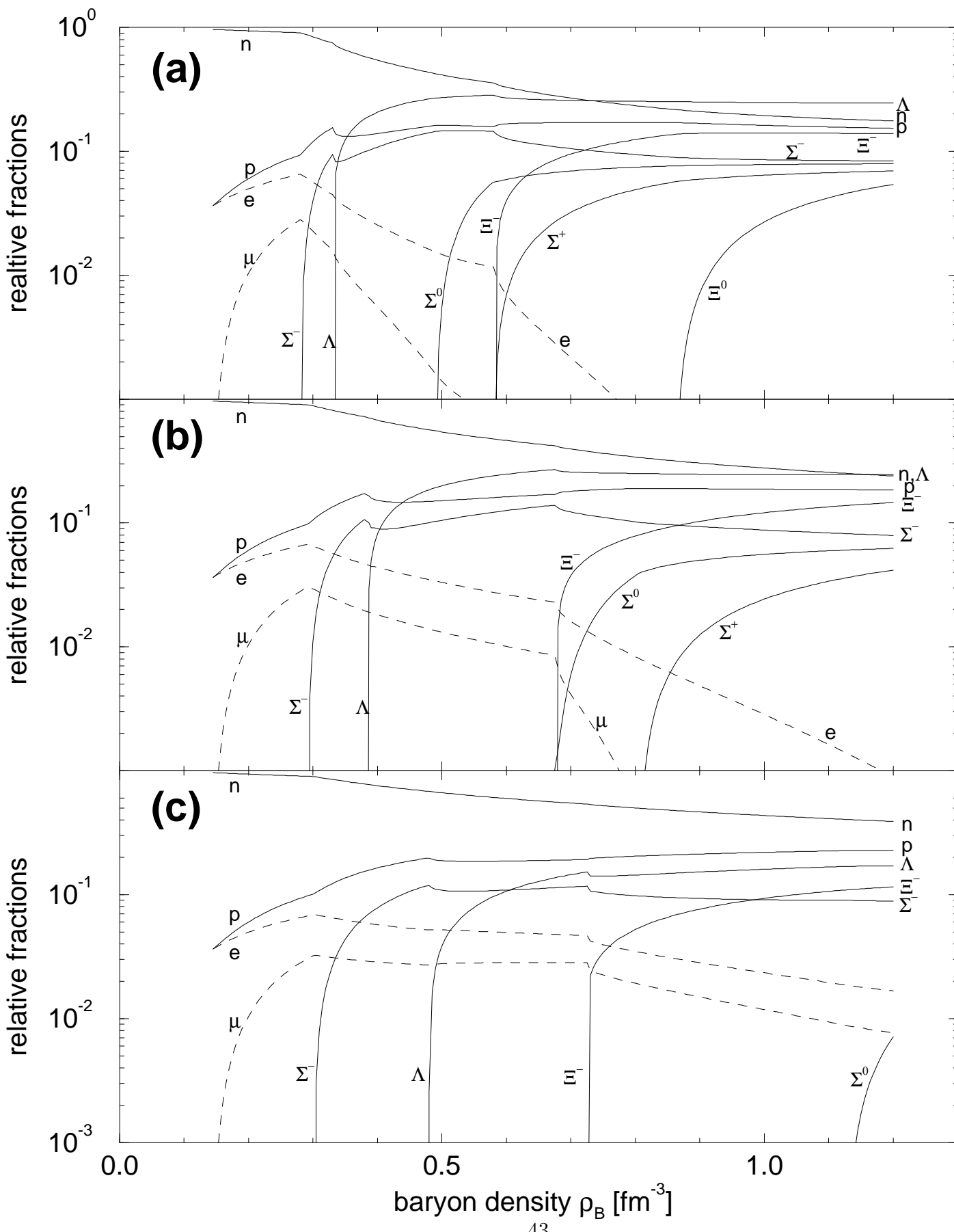


figure 4

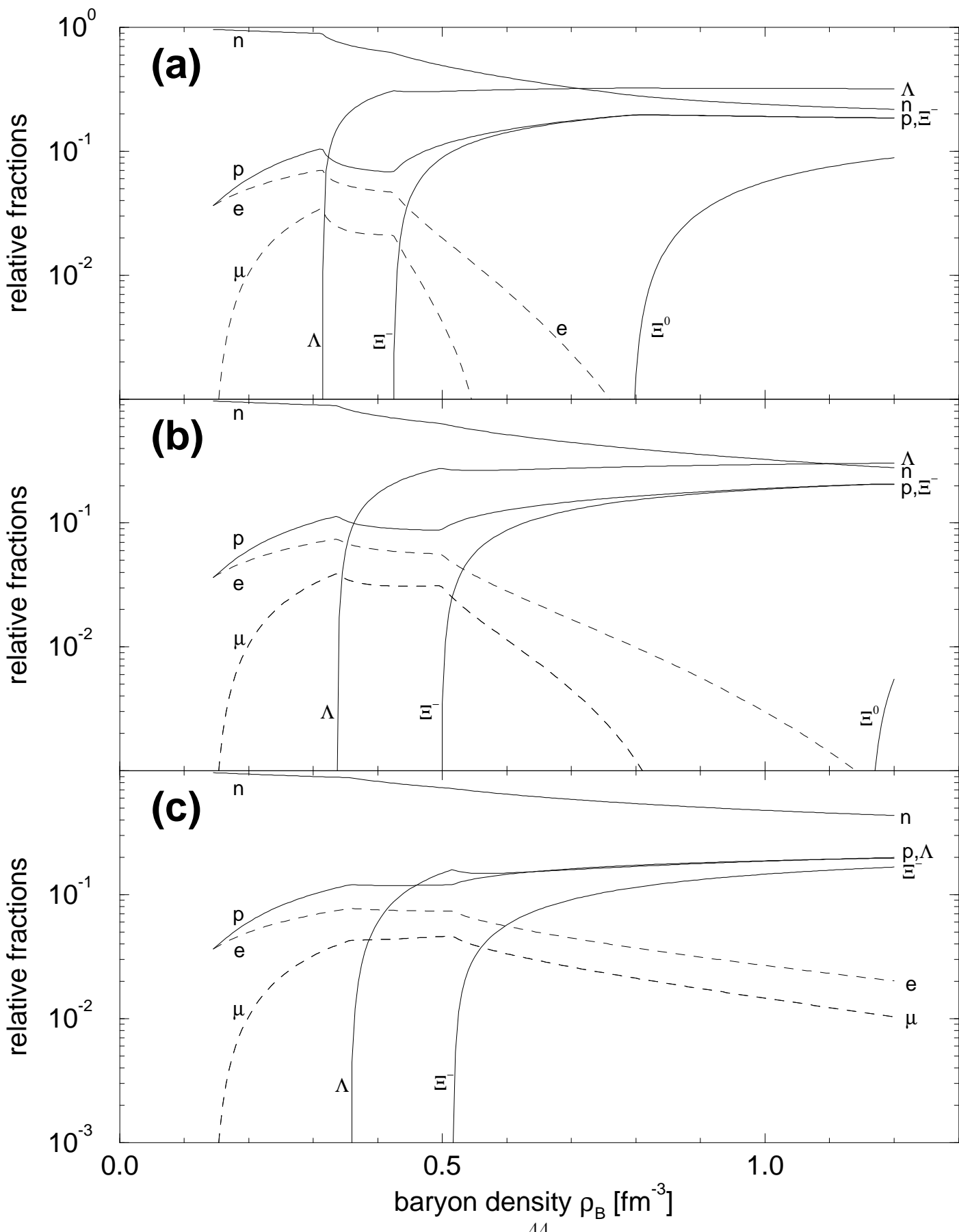


figure 5

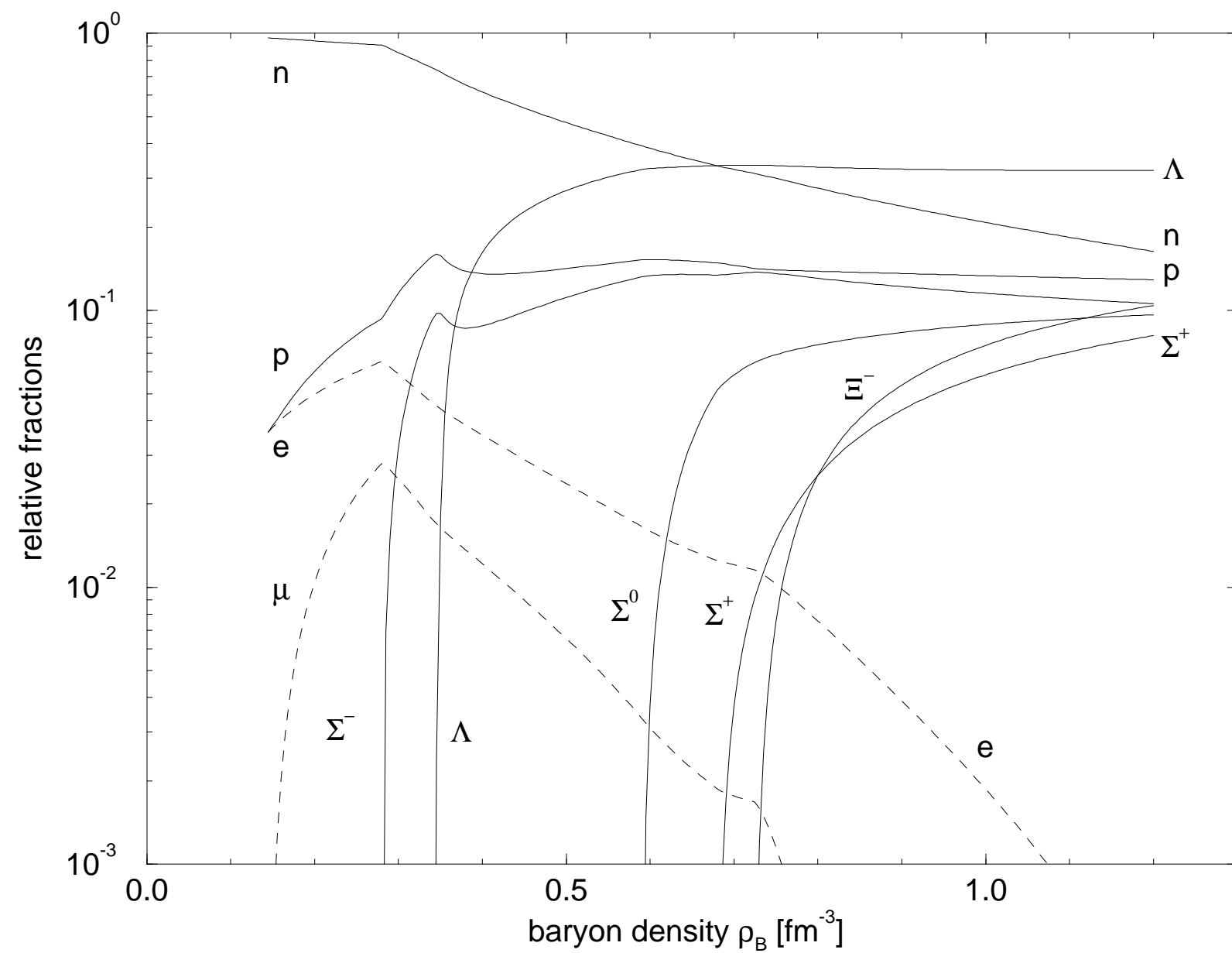


figure 6

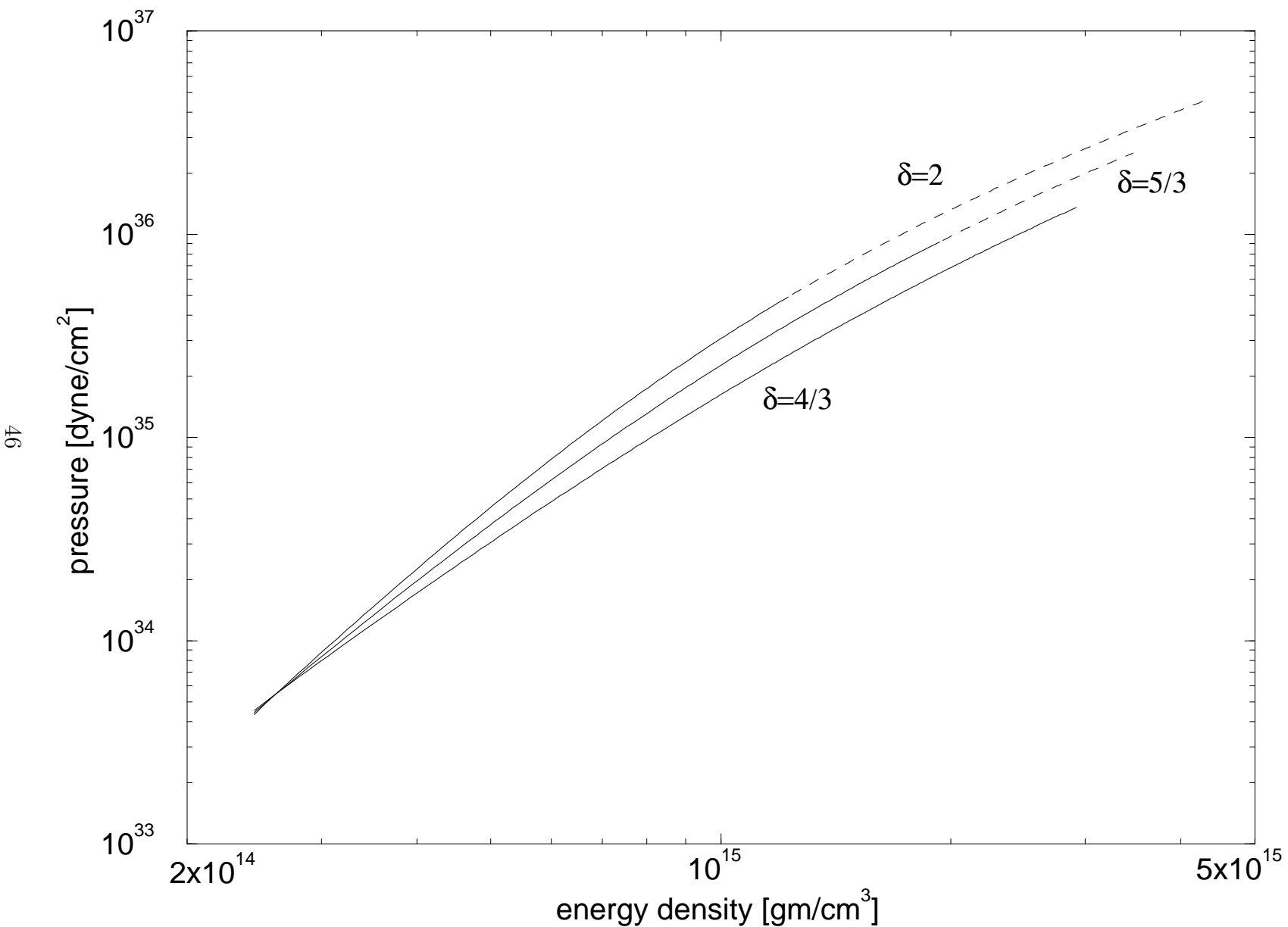


figure 7

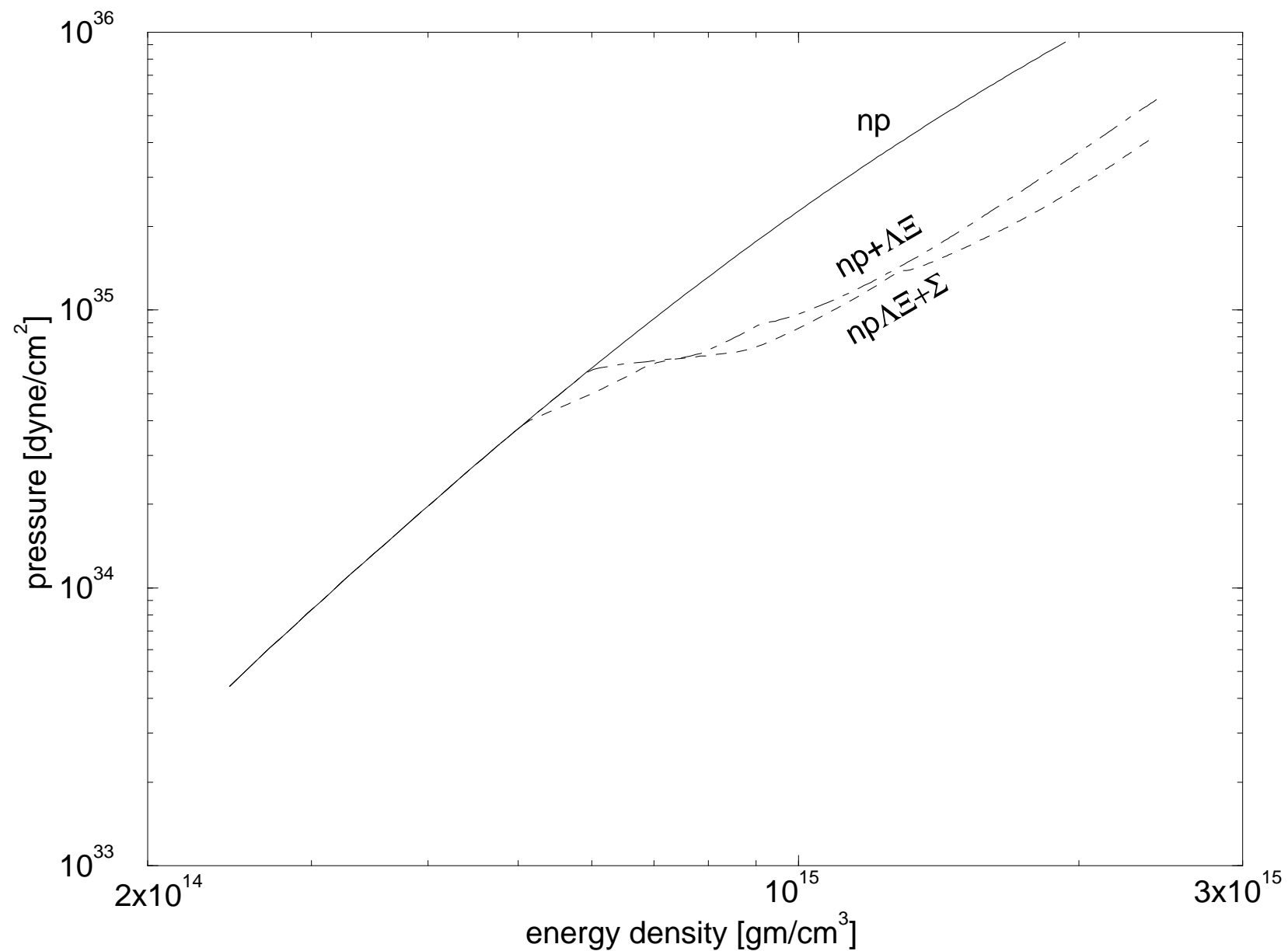


figure 8

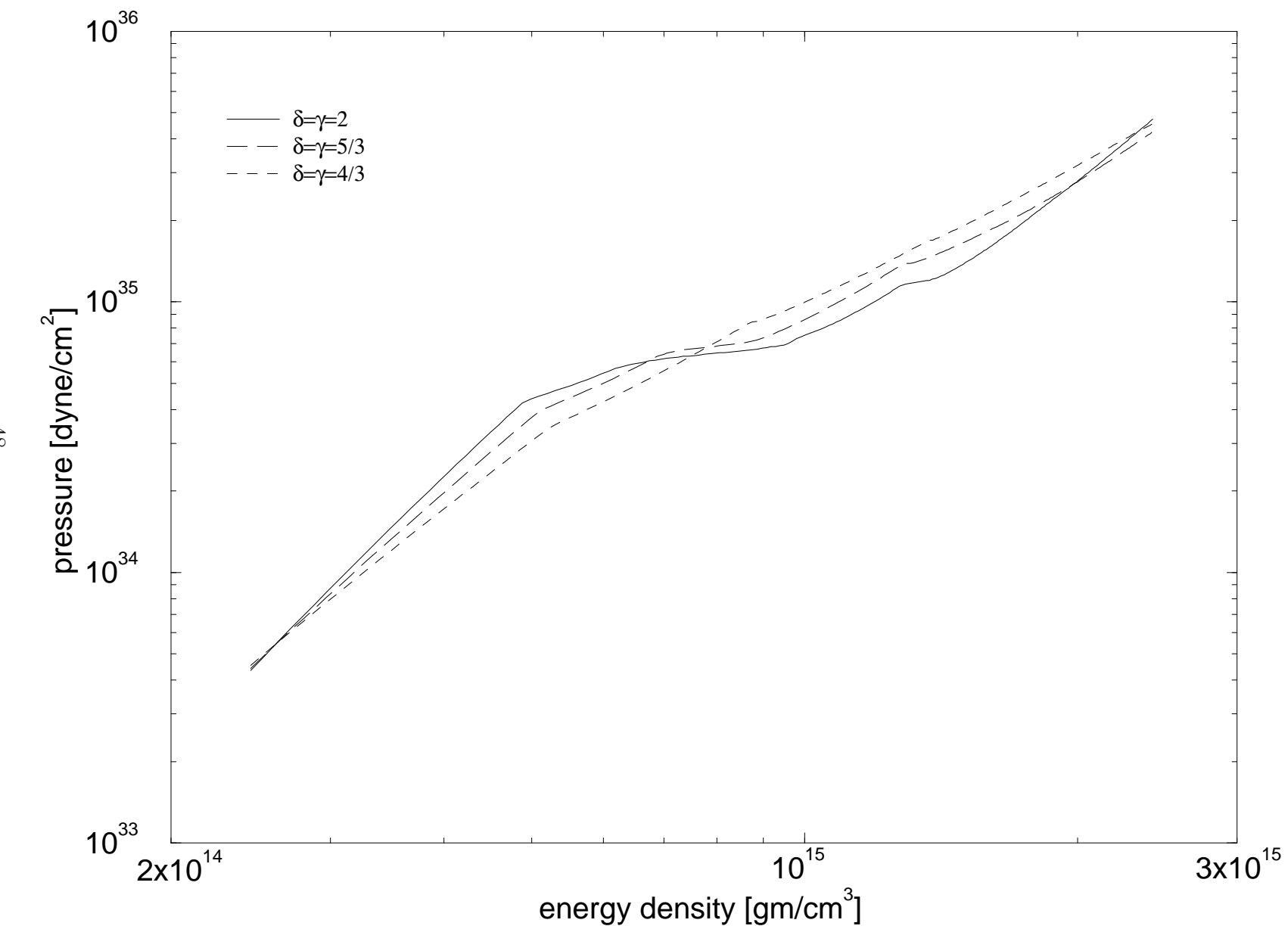


figure 9

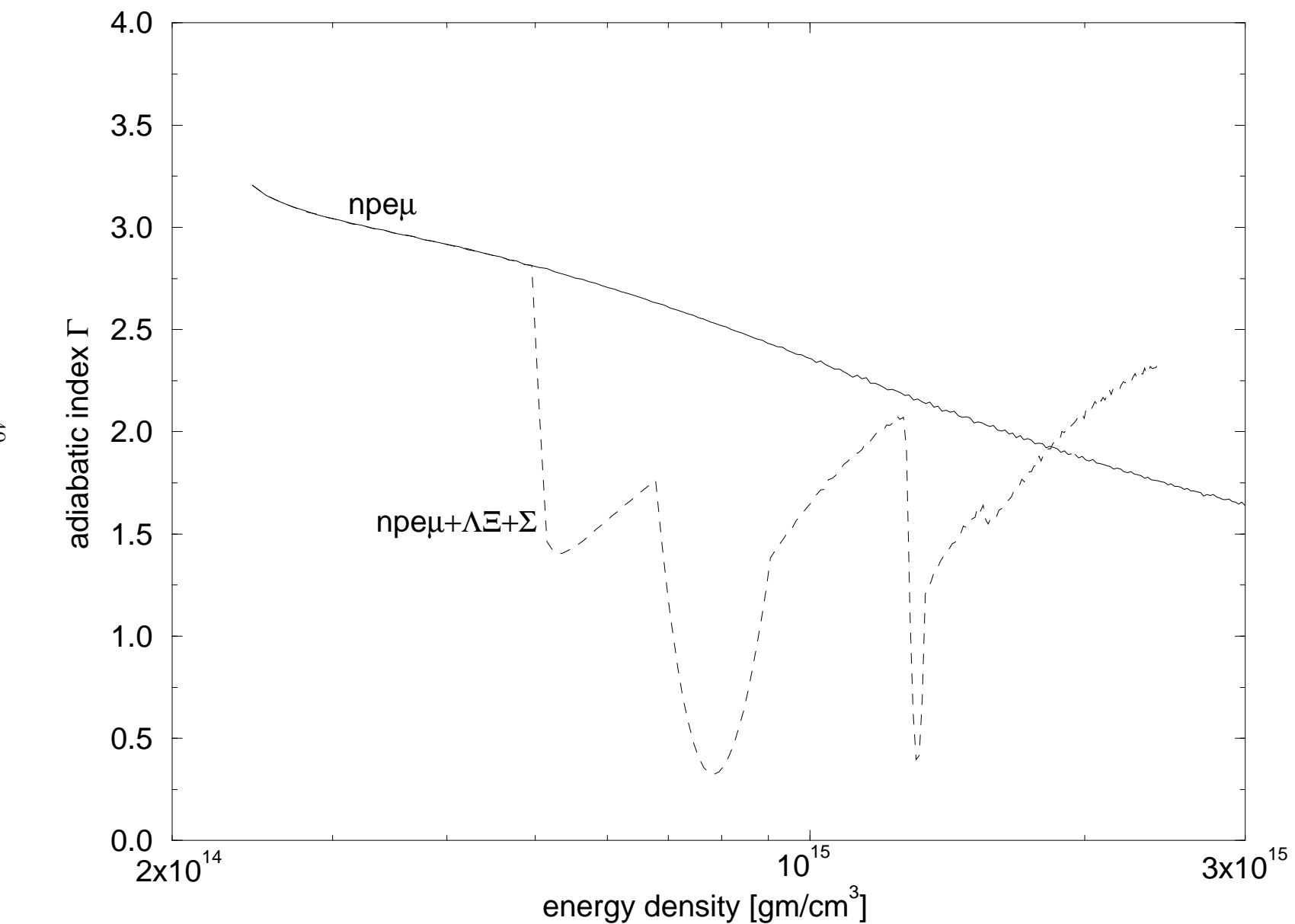


figure 10

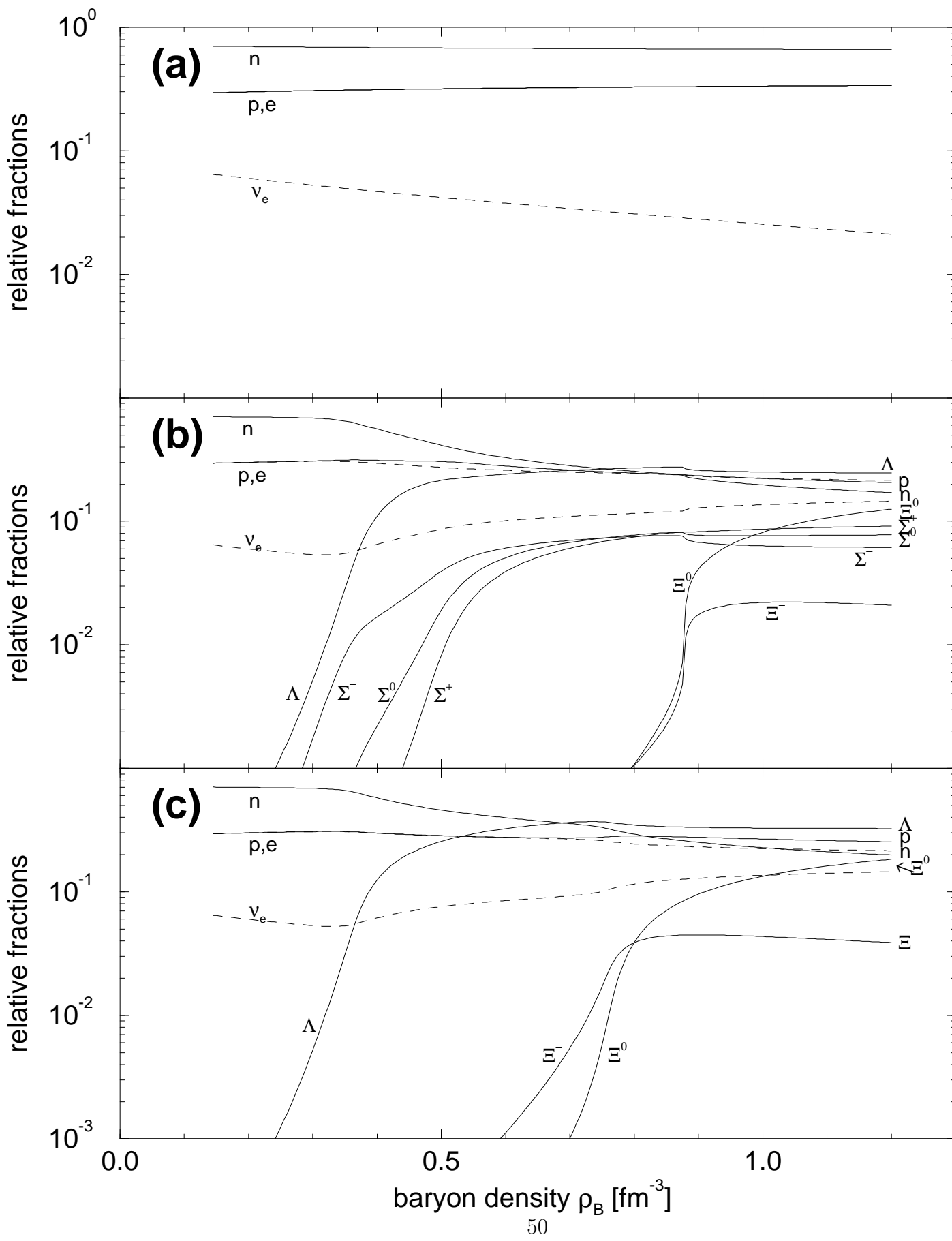


figure 11

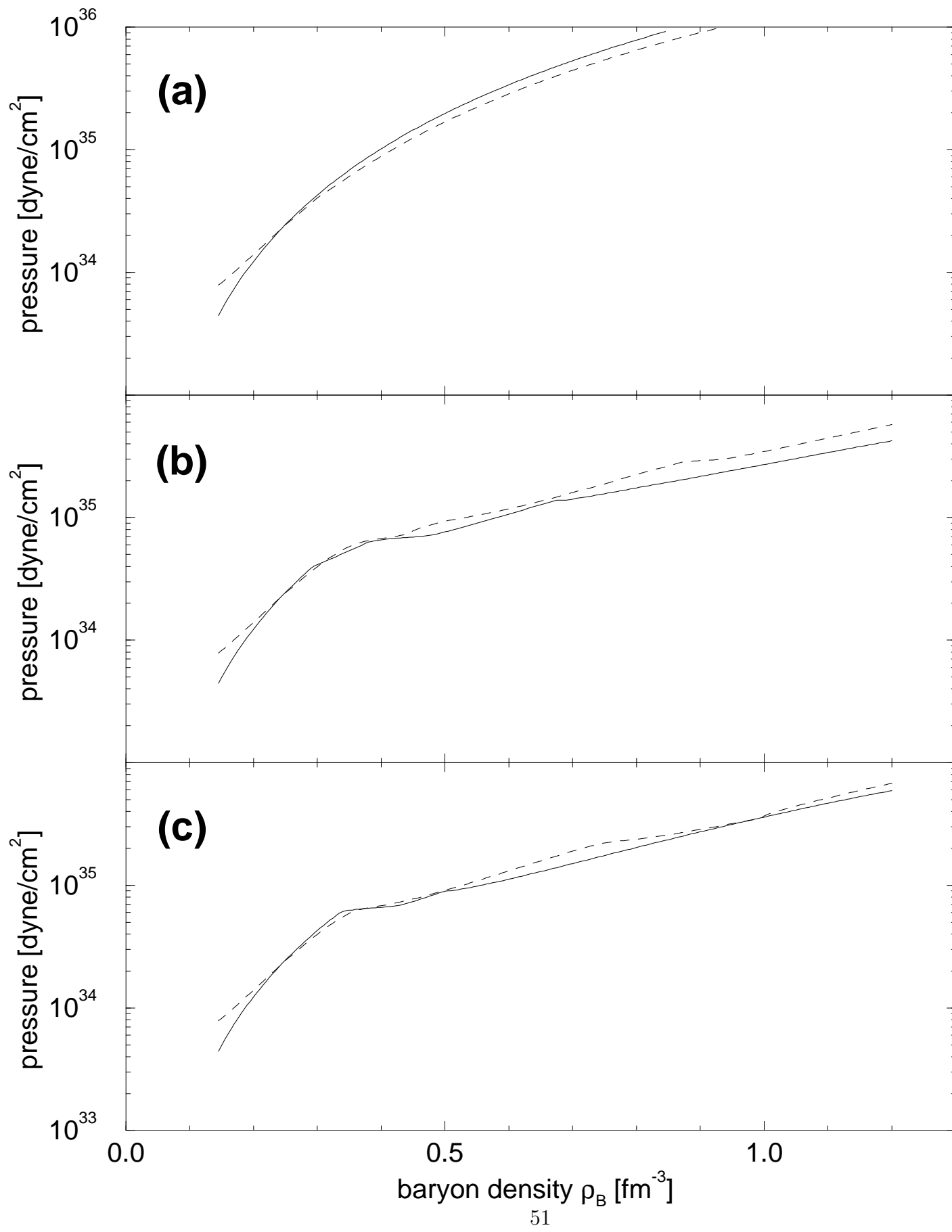


figure 12

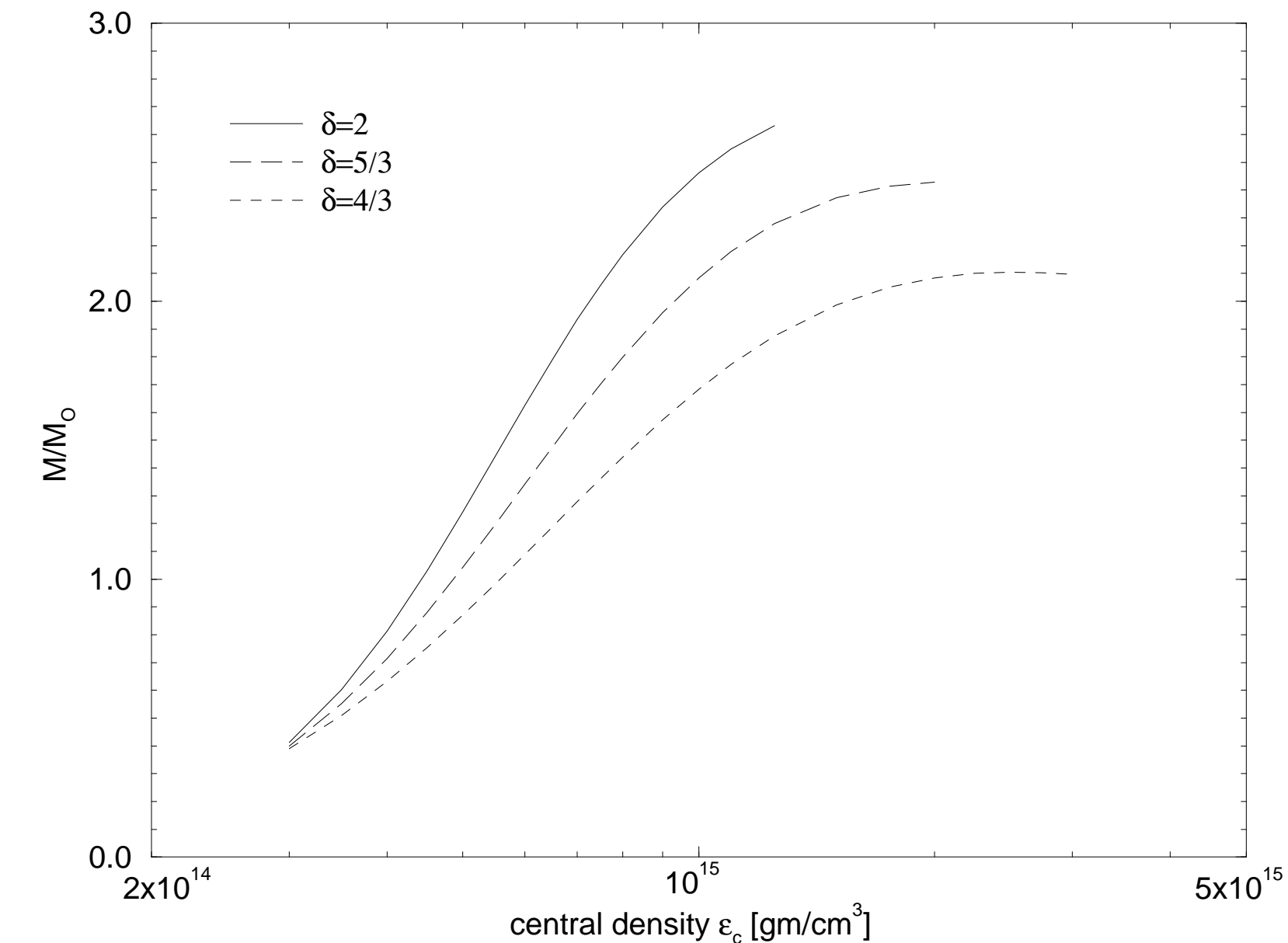


figure 13

